Available online at www.sciencedirect.com

ScienceDirect

Geochimica et Cosmochimica Acta 248 (2019) 370–386

Geochimica et Cosmochimica Acta

www.elsevier.com/locate/gca

Boron isotope systematics of cultured brachiopods: Response to acidification, vital effects and implications for palaeo-pH reconstruction

Hana Jurikova [a,*], Volker Liebetrau [a], Marcus Gutjahr [a], Claire Rollion-Bard [b], Marian Y. Hu [c], Stefan Krause [a], Daniela Henkel [a], Claas Hiebenthal [a], Mark Schmidt [a], Jürgen Laudien [d], Anton Eisenhauer [a]

[a] GEOMAR Helmholtz-Zentrum für Ozeanforschung Kiel, Wischhofstr. 1-3, 24148 Kiel, Germany
[b] Institut de Physique du Globe de Paris (IPGP), Sorbonne Paris Cité, Université Paris Diderot, UMR 7154 CNRS, 1 rue Jussieu, 75238 Paris, France
[c] Physiologisches Institut, Christian-Albrechts-Universität zu Kiel, Hermann-Rodewald-Str. 5, 24118 Kiel, Germany
[d] Alfred-Wegener-Institut Helmholtz-Zentrum für Polar- und Meeresforschung, Am Handelshafen 12, 27570 Bremerhaven, Germany

Received 17 April 2018; accepted in revised form 9 January 2019; available online 14 January 2019

Abstract

CO_2-induced ocean acidification and associated decrease of seawater carbonate saturation state contributed to multiple environmental crises in Earth's history, and currently poses a major threat for marine calcifying organisms. Owing to their high abundance and good preservation in the Phanerozoic geological record, brachiopods present an advantageous taxon of marine calcifiers for palaeo-proxy applications as well as studies on biological mechanism to cope with environmental change. To investigate the geochemical and physiological responses of brachiopods to prolonged low-pH conditions we cultured *Magellania venosa*, *Terebratella dorsata* and *Pajaudina atlantica* under controlled experimental settings over a period of more than two years. Our experiments demonstrate that brachiopods form their calcite shells under strong biological control, which enables them to survive and grow under low-pH conditions and even in seawater strongly undersaturated with respect to calcite (pH = 7.35, $\Omega_{cal} = 0.6$). Using boron isotope ($\delta^{11}B$) systematics including MC-ICP-MS as well as SIMS analyses, validated against *in vivo* microelectrode measurements, we show that this resilience is achieved by strict regulation of the calcifying fluid pH between the epithelial mantle and the shell. We provide a culture-based $\delta^{11}B$–pH calibration, which as a result of the internal pH regulatory mechanisms deviates from the inorganic borate ion to pH relationship, but confirms a clear yet subtle pH dependency for brachiopods. At a micro-scale level, the incorporation of boron appears to be principally driven by a physiological gradient across the shell, where the $\delta^{11}B$ values of the innermost calcite record the internal calcifying fluid pH while the composition of the outermost layers is also influenced by seawater pH. These findings are of consequence to studies on biomineralisation processes, physiological adaptations as well as past climate reconstructions.
© 2019 The Authors. Published by Elsevier Ltd. This is an open access article under the CC BY-NC-ND license (http://creativecommons.org/licenses/by-nc-nd/4.0/).

Keywords: Boron isotopic composition; Culturing experiment; Physiological response; Proxy calibration; Biomineralisation; Low-magnesium calcite; pH and pCO_2 reconstruction

1. INTRODUCTION

Brachiopods have survived multiple Phanerozoic crises since their radiation during the early Cambrian and still

* Corresponding author.
E-mail address: hjurikova@geomar.de (H. Jurikova).

https://doi.org/10.1016/j.gca.2019.01.015
0016-7037/© 2019 The Authors. Published by Elsevier Ltd.
This is an open access article under the CC BY-NC-ND license (http://creativecommons.org/licenses/by-nc-nd/4.0/).

today present widespread taxa (e.g. Carlson, 2016). They are abundant in the marine fossil record, and owing to their good preservation they have been increasingly used to assess past changes of ocean chemistry and climate state (e.g. Veizer et al., 1999; Farkaš et al., 2007; Brand et al., 2012, Vollstaedt et al., 2014; Garbelli et al., 2017). Their shell composed of low-magnesium calcite makes them more resistant to post-depositional alteration of primary chemical signals and potentially an advantageous geochemical palaeo-archive (e.g. Brand and Veizer, 1980; 1981; Brand et al., 2003). Yet to date, brachiopod proxy relationships have been barely examined under controlled laboratory conditions, and in contrast to other marine calcifiers such as corals or foraminifera (e.g. Rollion-Bard et al., 2003; McCulloch et al., 2012a,b; Raddatz et al., 2014; Tanaka et al., 2015; Taubner et al., 2017; Jurikova et al., 2019) surprisingly little is known on the mechanisms that control the incorporation of various key elements and isotope systems into brachiopod calcite. Whereas the lack of culture-based studies poses an uncertainty for accurate interpretation of palaeo-records, it also limits our understanding of the biological processes that may have enabled brachiopods to endure strong environmental changes, which will be tested under rising anthropogenic pressures (such the present threat from CO_2-induced ocean acidification).

The boron isotope ($\delta^{11}B$) composition of biogenic carbonates is considered to be one of the most reliable pH-proxies (e.g. Vengosh et al., 1991; Hemming and Hanson, 1992; Sanyal et al., 2000) as it reflects the pH of fluid from which it precipitated. Although this is primarily seawater, several organisms have been found to be able to modify internal chemistry at the site of calcification (Al-Horani et al., 2003; de Nooijer et al., 2009; Stumpp et al., 2012; Anagnostou et al., 2012; McCulloch et al., 2012a,b; Venn et al., 2013; Ramesh et al., 2017) as a result of active ion transport and precipitation under non-equilibrium conditions termed 'vital effects', complicating the interpretation and calibration of $\delta^{11}B$ data (Rollion-Bard and Erez, 2010). Calibrations based on $\delta^{11}B$ analyses of samples from known pH environments have enabled an evaluation of the extent of vital effects on $\delta^{11}B$. The latter has become relatively well established for foraminifera (e.g. Henehan et al., 2013; 2016), and to some degree for corals (e.g. Trotter et al., 2011), allowing new insights into perturbations of the marine carbon cycle (e.g. Gutjahr et al., 2017) and even species-specific pH-regulating capacities (e.g. McCulloch et al., 2012b; Ross et al., 2018). However, the use of these two groups is mainly limited to the Cenozoic; their insufficient preservation and availability limits their use for geological time scales predating the Cenozoic for which an alternative archive is needed. For this, brachiopods represent highly suitable candidates, provided that a preceding careful assessment of vital effects can be made. Moreover, detailed $\delta^{11}B$ examination may permit us to illuminate their pH-controlling mechanism, a key but not universally developed ability of calcifiers to withstand ocean acidification. So far, only few studies focused on the potential of brachiopods as $\delta^{11}B$–pH recorders (Lécuyer et al., 2002; Joachimski et al., 2005; Penman et al., 2013). Relationship between brachiopod $\delta^{11}B$ and ambient pH has been postulated by Lécuyer et al. (2002) and Penman et al. (2013) based on co-variations of $\delta^{11}B$ from natural samples and oceanic regimes with distinct seawater pH. These calibrations may, however, potentially involve large uncertainties as the role of a sole parameter on the calcite chemistry is likely to be obscured or hampered by additional unknowns such as environmental parameters, growth rates or internal vital effects.

In order to provide a systematic understanding of boron incorporation into brachiopod calcite, assess their potential as palaeo-archives, and decipher the role of vital effects, we investigated the $\delta^{11}B$ composition of three brachiopod species; *Magellania venosa* (Dixon, 1789), *Pajaudina atlantica* Logan, 1988 and *Terebratella dorsata* (Gmelin, 1791). Brachiopod specimens were cultured under controlled experimental settings comprising different pCO_2 and thus pH treatments. Solution-based MC-ICP-MS (Multicollector-Inductively Coupled Plasma-Mass Spectrometer) analyses were used to establish a culture-based $\delta^{11}B$–pH calibration, discuss its implications for palaeo-pH and palaeo-CO_2 reconstructions, and to approximate the extent of vital effects involved. Further, we carried out high spatial resolution SIMS (Secondary Ion Mass Spectrometry) measurements to study intrashell $\delta^{11}B$ variations and their link to biomineralisation. Finally, we performed *in vivo* calcifying fluid pH measurements using microelectrodes, to our knowledge the first of its kind for brachiopods, to reconcile the interpretation of $\delta^{11}B$-related vital effects in the context of internal pH-regulating capacities, and to corroborate whether boric acid may in part be also incorporated into brachiopod calcite (Klochko et al., 2009; Noireaux et al., 2015; Mavromatis et al., 2015; Balan et al., 2018).

2. MATERIALS AND METHODS

2.1. Brachiopod sites and sampling

We cultured three different brachiopod species over the period of approximately two years under controlled experimental settings in a climatically controlled laboratory (of the KIMOCC – Kiel Marine Organism Culture Center) at GEOMAR in Kiel, Germany. Specimens of the cold-water species *M. venosa* (Fig. 1a), the largest living brachiopod, were harvested from three sites in the Comau Fjord in Chilean Patagonia (Jetty 42°22′47″S, 72°24′56″W, Cross–Huinay 42°23′28″S, 72°27′27″W, and Liliguapy 42°9′43″S, 72°35′55″W) at 21 m depth. We also found few *T. dorsata* (Fig. 1b), a commonly associated brachiopod species with *M. venosa*, and co-cultured them together with *M. venosa*. The Comau Fjord encompasses a 41 km long, 4.5 km wide and 487 m deep basin, and presents an oceanographically and ecologically well-studied area (Sievers and Silva, 2008a,b,c; Häussermann and Försterra, 2009; Pantoja et al., 2011). The fjord is characterized by strong vertical stratification, with fairly homogenous temperatures below the surface layer of 8–12 °C, salinity about ~ 30 (Baumgarten et al., 2013) and pH of 7.8–8.0 at 20 m depth (Jantzen et al., 2013). *M. venosa* is an abundant species in the fjord and all throughout Southern Patagonia, and is

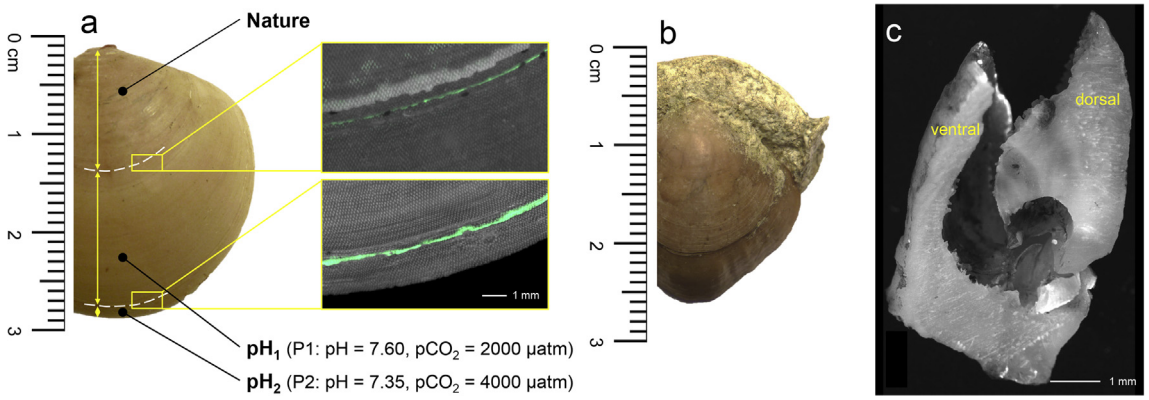

Fig. 1. (a) *Magellania venosa* specimen (dorsal valve) cultured under low-pH/high-pCO_2 conditions. Respective parts of the shell precipitated under natural vs. culture conditions (pH_1 and pH_2) are indicated by dashed white lines, and correspond to external growth marks on the shell as well as to the fluorescent calcein marker (green lines showed in enlarged microscope images. (b) *T. dorsata* (dorsal valve) from a control treatment. (c) Section through a *P. atlantica* specimen cultured under low-pH/high-pCO_2 conditions. Neither the calcein marker nor culture growth bands are discernible for this species. (For interpretation of the references to colour in this figure legend, the reader is referred to the web version of this article.)

found attached to hard substrates of the shallow subtidal zone to 2000 m depth (McCammon, 1973).

Specimens of the warm-water species *P. atlantica* (Fig. 1c) were collected attached to rocks (app. 60 to 80 individuals per rock) at 18 m depth from La Palma, Canary Islands (Punta Malpique 28°27′17″N, 17°50′40″W). *P. atlantica* inhabit hard substrates of caves and shaded overhangs where they are found cemented to the substrate in great numbers up to 5000 individuals m^{-2} (Álvarez et al., 2005; Logan, 2004). While the physical conditions of the surface ocean are driven by seasonal variations, with a temperature range between 17–26 °C throughout the year (Giumerans and Cañavate, 1994), the crevices colonised by *P. atlantica* likely see only narrow oscillations. In January 2016 we measured temperature of ~21 °C, salinity of ~36, and pH ~8.1.

2.2. Culturing and experimental setup

The environmental conditions in our experimental culturing tanks simulated the natural conditions (as detailed in the previous Section 2.1) for both cold- and warm-water species. Prior to the start of the experimental treatments, brachiopods transported from the field remained in an acclimatisation phase at control conditions for five and seven weeks for *M. venosa* and *P. atlantica*, respectively. To monitor the newly grown shell material, all brachiopods were marked using fluorescent calcein (©Sigma-Aldrich) dye (Riascos et al., 2007; Baumgarten et al., 2012); *P. atlantica* were kept in calcein stained water (1 g of calcein per 10 L of water, buffered with NaOH to ambient pH) for seven days, *M. venosa* and *T. dorsata* for 24 h. As culture medium (hereinafter CM) we used artificial seawater that was prepared by mixing Tropic Marin Pro-Reef commercial sea-salt (Atkinson and Bingman, 1998) with deionised water until the desired salinity and elemental concentrations were achieved (Table 1). Each brachiopod-culturing aquarium sized 150 L and acted as a semi-closed system with separate water cycle. Fresh CM with matching salinity and chemical composition was supplied from a reservoir tank. Twice a month 10% of the CM in the brachiopod-culturing aquarium was replaced with new CM from the reservoir tank to remove the metabolites from the system, following the established protocols and experiences at KIMOCC. Deionised water was automatically added to the aquariums to compensate for evaporated water volume. The CM temperature was controlled using heaters or coolers (depending on the treatment) from Aqua Medic and maintained at stable conditions (see Table 1). Experimental cultures used in the present study were kept at 22 ± 1 °C for *P. atlantica*, and 10 ± 1 °C for *M. venosa* and *T. dorsata*. A biofilter, protein skimmer and UV sterilizer were used for CM filtering. All aquariums were equipped with calibrated automated sensors for continuous measurements of salinity (Conductivity Electrode), temperature (Temperature Sensor Aquarium for *P. atlantica* and Temperature Sensor Pond for *M. venosa* aquariums) and pH (pH-Electrode) connected to a GHL ProfiLux aquarium computer 3.1T eX (Kaiserslautern, Germany) for data storing, which were validated against manual measurements several times per week. An optical membrane-inlet CO_2 sensor (CONTROS HydroC® underwater CO_2 sensor; Kongsberg Maritime Contros GmbH, Kiel, Germany) calibrated for a pCO_2 range of 200–6000 µatm (with accuracy ~1% of reading; Fietzek et al., 2014) was used for continuous monitoring of the pCO_2 in the aquariums as well as the CO_2 in the room air.

Additionally, CM from all brachiopod-culturing aquariums, reservoir tanks, and deionised water source was routinely (roughly every month) sampled and analysed for major and trace element content, isotopic composition, total alkalinity (TA) and total dissolved inorganic carbon (DIC) content. Total alkalinity was determined immediately after water sampling via open-cell titration of 0.5 ml samples with 0.01 M HCl in a titration vessel after Pavlova et al. (2008) using a Metrohm 876 Dosimat plus (Ω Metrohm, Florida, USA). During titration, the vessel

Table 1
Experimental culturing settings, seawater and carbonate system parameters (±1σ long-term variations throughout the duration of the corresponding culturing treatments). During CO_2 phase 2 (P2) the CO_2 partial pressure in aquarium B1 ($pH_{1/2}$ to pH_2) and C3 (pH_1 to pH_2) was increased to 4000 µatm.

Aq. No.	Treatment	ID	Species	Sal. ±0.05	T [°C] ±1	pCO_2 [µatm] ±10%	pH ±0.05	TA [mmol/l] ±0.3	DIC [mmol/l] ±12%	Ω_{cal}
CO_2 phase 1 (P1): August 2016–April 2017										
A1	Control	pH_0	*P. atlantica*	36	22	600	8.20	3.2	2.6	9.9
A3	pCO_2	pH_1	*P. atlantica*	36	22	2000	7.70	3.4	2.7	4.6
B1	pCO_2	$pH_{1/2}$	*P. atlantica*	36	22	1500	7.80	3.3	3.5	4.8
C2	Control	pH_0	*M. venosa*	30	10	600	8.00	2.3	2.0	2.0
C3	pCO_2	pH_1	*M. venosa*	30	10	2000	7.60	2.8	2.7	1.1
CO_2 phase 2 (P2): April 2017–July 2017										
A1	Control	pH_0	*P. atlantica*	36	22	600	8.25	3.8	2.6	10.4
A3	pCO_2	pH_1	*P. atlantica*	36	22	2000	7.70	3.3	2.8	3.9
B1	pCO_2	pH_2	*P. atlantica*	36	22	4000	7.35	3.5	3.1	2.0
C2	Control	pH_0	*M. venosa*	30	10	600	8.15	2.9	2.9	3.5
C3	pCO_2	pH_2	*M. venosa*	30	10	4000	7.35	3.1	3.5	0.6

was continuously purged with N_2 to strip CO_2 released by acid addition. All TA measurements were calibrated with IAPSO seawater standard and had an accuracy of 5%. For DIC measurements, 1 ml of filtered water sample (28 mm diameter, SFCA membrane, 0.2 µm mesh size) was transferred into a CO_2-free 10 ml glass vial and sealed. Subsequently, 100 µl of 6 M HCl was added. After minimum of 6 h of equilibration time 100 µl of gas headspace was measured using a gas chromatograph (Shimadzu) equipped with a methanizer. DIC measurements were calibrated with bicarbonate solutions of concentrations ranging from 0 to 25 mM and an IAPSO seawater standard, and had an accuracy of 5%. The CM samples for elemental and isotopic analyses were collected in 4 ml vials using syringe filters (28 mm diameter, SFCA membrane, 0.2 µm mesh size), acidified (40 µl concentrated HNO_3 for the total volume of 4 ml), and stored in a refrigerator room at 4 °C until analysis. Calcite saturation state (Ω_{cal}) was calculated according to Zeebe and Wolf-Gladrow (2001).

In total five different culturing aquariums were used for this study consisting of control (A1) and two low-pH (A3 and B1) treatments for *P. atlantica,* as well as a control (C2) and a low-pH treatment (C3) for *M. venosa* and *T. dorsata* (Table 1). The control treatments simulated typical natural conditions for each brachiopod species. The pCO_2 in control treatments was 600 µatm, matching the room air concentration, which is expected due to reduced air circulation in the enclosed climate laboratory. Elevated pCO_2 levels in the low-pH experimental treatments (A3, B1 and C3) were achieved by continuous bubbling of CO_2-enriched air through an air stone, which we found to be more effective than via a skimmer. We started culturing *P. atlantica* in January 2016 and *M. venosa* in May 2016. Carbon dioxide-mediated acidification experiments were initiated in August 2016; during the first CO_2 phase (P1) from August 2016 until April 2017 aquariums A3 and C3 were maintained at 2000 µatm pCO_2 ($pH_1 = 7.7$ and 7.6, respectively; Table 1), and aquarium B1 at moderate 1600 µatm pCO_2 ($pH_{1/2} = 7.8$); the second CO_2 phase (P2) begun in April 2017 during which pCO_2 was elevated to 4000 µatm in aquariums B1 and C3 ($pH_2 = 7.35$ for both). Samples for the present study were harvested in July 2017. The 4000 µatm CO_2 experiments ended in June 2018. Overall, the brachiopods appeared to thrive in all treatments, and we observed only low mortality rates throughout (<10%) associated to transport stress rather than the culturing conditions. For calcein imaging a Zeiss stereomicroscope Discovery.V8 was used. Images were obtained with a Zeiss AxioCam MRm Rev 3 and processed using the Zen 2.3 SP1 software.

2.3. Sample preparation

Brachiopod shells were gently rinsed with ultra pure water (Milli-Q), and dried over few days on a hotplate at 40 °C in a laminar flow hood. Targeted growth increments precipitated under specific experimental conditions (Fig. 1) were sub-sampled for mini-bulk analyses under binoculars using a precision drill (Proxxon) with dental tips (~100 µm diameter). Approximately 1–3 mg of $CaCO_3$ powder was collected in 1.5 ml centrifuge vials, integrating a shell growth interval of about one to two months. Powders were rinsed with Milli-Q followed by an oxidative cleaning procedure (following Barker et al., 2003) during which organic matter was oxidised with 1% hydrogen peroxide buffered with 0.1 M ammonium hydroxide at 80 °C (approximately 250–500 µl of oxidative mixture was used per sample). Cleaned samples were subsequently transferred into 1.5 ml centrifuge Teflon vials and treated with 0.5 mM HNO_3 (typically 250 µl per sample) for 30 seconds to remove any adsorbed contaminants (following Foster, 2008) Finally, we dissolved the samples in 0.5 M HNO_3 with the aid of ultrasonication (depending on sample size, approximately 100–200 µl of 0.5 M HNO_3 was required to achieve complete dissolution). An aliquot of 10% of each dissolved sample was analysed for major and trace elements (Li, B, Na, Mg, Ca, Sr, and Ba; for the present study only B and Ca are relevant, to fully explore all major and trace element data is beyond the scope of this manuscript and will be presented in a separate publication) using a Quadrupole ICP-MS (Agilent 7500x) at GEOMAR, Kiel. The long-term external reproducibility RSD (relative standard deviation,

2σ) was better than 3% for B/Ca assessed by repeated measurements of carbonate reference materials JCp-1, JCt-1 and our in-house brachiopod standard MVS-1.

Culture medium samples were measured for major and trace elements (Li, B, Na, Mg, K, Ca, Sr, and Ba) with an ICP-OES (Inductively Coupled Plasma-Optical Emission Spectrometry) The long-term external reproducibility RSD (relative standard deviation, 2σ) was better than 2% for B/Ca determined by repeated measurements of IAPSO standard seawater.

Prior to boron isotope analysis, boron is separated from the sample's carbonate matrix on micro-columns (25 µl volume) using boron specific anionic exchange resin Amberlite IRA 743 crushed and sieved to 63–120 µm (Kiss, 1988; Lemarchand et al., 2002a). Samples were buffered to a pH of 5 using 2 M sodium acetate−0.5 M acetic acid buffer (typically twice the amount of buffer than the dissolution 0.5 M HNO_3 is required) and carefully loaded on the chromatographic columns. Boron retention on the resin is pH dependent (see Lemarchand et al., 2002a); thus repeated rinses with Milli-Q water were necessary to elute the carbonate matrix and the buffer, while purified boron was collected with 720 µl of 0.5 M HNO_3. All columns were individually calibrated with yields verified by a highly resolved elution scheme (consisting of minimum 30 steps), yielding >98% boron recovery. To ensure that no significant amount of the sample remained on the column, boron content of each elution tail was determined representing <1% of the total boron in the sample. Likewise, a total procedural blank (TPB) for each column batch was determined; all TPBs were below <100 pg (<0.1% of the sample size, n = 12). Purified boron samples were stored in Teflon vials and diluted to 35 ppb before analysis using 0.5 M HNO_3, and based on previous B concentration assessments on the Quadrupole ICP-MS.

2.4. Boron isotope analyses on MC-ICP-MS

The boron isotopic composition of brachiopod $CaCO_3$ and CM was determined at GEOMAR, Kiel on a Thermo Scientific Neptune Plus MC-ICP-MS following procedures outlined in Foster (2008) with modifications. Prior to each analysis the instrument was tuned for maximum $^{11}B/^{10}B$ stability. We used an ESI PFA 50 µl min^{-1} nebuliser and a Teflon barrel spray chamber. We did not find any significant improvement in washout when running the instrument with ammonia add gas; on the contrary, the addition of ammonia led to precipitation of ammonium nitrate in the Teflon spray chamber and the injector, thereby requiring cleaning of the sample introduction unit after each ~24 h of running. Machine-induced mass fractionation was corrected by standard-sample bracketing with a 35 ppb standard NIST SRM 951 boric acid that consequently converts $^{11}B/^{10}B$ ratios to delta notations. We aimed for matched sample to standard concentration, although within the range of ~10 to 50 ppb boron per sample the required precision and accuracy was achieved. Each analysis consisted of 120 seconds lasting simultaneous collection of masses 11 and 10 with Faraday cups H4 and L4 (both with 10^{12} Ω resistors), respectively. The typical signal intensity was 10–20 mV per 1 ppb on mass 11. Each sample was analysed twice during each analytical session with the average value reported. Airborne boron contamination to the open sample vials in the autosampler caused significant blank accumulation. In order to obtain the best possible control over the boron memory in the spray chamber, an on-peak zero was run over 30 seconds immediately preceding the take-up of the following sample or standard containing the same volume of 0.5 M HNO_3 (typically 1.5 ml). Following this protocol background blank contribution as high as 10% could be corrected without significant negative impact on either the standard or the sample composition as quantified with secondary standards run under identical conditions throughout sequences. This allowed for a maximum length of one analytical session of approximately 11 h during which a sequence of 10 samples, 6 standards and corresponding 16 blanks were measured twice (total of 32 positions in the autosampler). The external reproducibility for $\delta^{11}B$ values was better than ±0.2‰ (2σ) assessed by repeated measurements of purified coral standard reference material JCp-1 [Okai et al. (2002); n = 15, $\delta^{11}B = 24.41 \pm 0.18$‰; in agreement with the certified value and other laboratories e.g. Aggarwal and You (2016)] and in-house *M. venosa* brachiopod standard MVS-1 (n = 46, $\delta^{11}B = 15.95 \pm 0.19$‰). The long-term Neptune Plus stability and performance was monitored by regular measurements of pure boron BAM reference materials (Vogl and Rosner, 2001), resulting in −20.31 ± 0.28‰ (n = 58); 19.70 ± 0.20‰ (n = 123); and 39.67 ± 0.22‰ (n = 104) for ERM-AE120, ERM-AE121 and ERM-AE122, respectively (between years 2016–2018).

2.5. Boron isotope analyses by SIMS

High spatial resolution boron isotopic analyses were performed at CRPG-CNRS, Nancy using Cameca IMS 1270 ion microprobe. The analytical settings are described in Blamart et al. (2007). In summary, a primary mass-filtered beam of $^{16}O^-$ ions with an intensity of 60–70 nA was focused into an aperture-delimited spot of approximately 40 µm using Kohler illumination. The analyses were conducted in a mono-collection mode on an electron multiplier by peak jumping between mass 9.8 (background), ^{10}B and ^{11}B. The deadtime of the electron multiplier was set at the beginning of the analytical session. The typical ion intensity on the samples was approximately 6000–20,000 counts s^{-1} for ^{11}B, for both natural and cultured brachiopod shells. Pre-sputtering to avoid any surface contamination lasted 2 minutes. Each measurement consisted of 60 cycles, with an acquisition time of 2 seconds for background, 12 seconds for ^{10}B, and 6 seconds for ^{11}B per cycle. The internal precision was approximately 0.6‰ (1σ), the average external reproducibility evaluated from replicate measurements of the in-house carbonate reference material WP22 (22 ppm B, $\delta^{11}B = 17.8$‰, vs. NIST SRM 951; Rollion-Bard et al., 2003, 2017) was ±1‰ (1σ). Accuracy and precision was additionally monitored by repeated measurements in the natural shell parts of *M. venosa*

($\delta^{11}B = 16.0‰$; see Section 2.4 above, which is a well established value as it is also our standard for solution-based analyses MVS-1) in-between measurements of the shell parts grown in the cultures.

2.6. Boron isotope systematics

Boron has two isotopes, ^{10}B and ^{11}B (approximately 20% and 80% of total B, respectively), and the $^{11}B/^{10}B$ variations are expressed in the standard delta notations in per mille (‰) relative to the reference material NIST SRM 951 boric acid (Catanzaro et al., 1970) as follows:

$$\delta^{11}B(‰) = [(^{11}B/^{10}B_{sample})/(^{11}B/^{10}B_{standard})^{-1}] \times 1000 \quad (1)$$

The principle of the $\delta^{11}B$ proxy is based on the speciation of boron in seawater. Boron is present in seawater almost exclusively as trigonal boric acid [$B(OH)_3$] and tetrahedral borate ion [$B(OH)_4^-$]. The relative proportion of boron species is pH dependent as defined by the following equilibrium:

$$B(OH)_3 + H_2O \leftrightarrow B(OH)_4^- + H^+. \quad (2)$$

Because of the differences in coordination and the subsequent B-O bond vibrational frequencies, an isotopic fractionation exists between the two species. Thus, as the distribution of boric acid and borate ion change with pH, so does their isotopic composition. The associated isotopic fractionation may be described as:

$$^{10}B(OH)_3 + {}^{11}B(OH)_4^- \leftrightarrow {}^{11}B(OH)_3 + {}^{10}B(OH)_4^-, \quad (3)$$

where the equilibrium constant $^{11-10}K_B$ (also termed as α_{4-3} or α_B in the literature) is defined as:

$$^{11-10}K_B = \frac{[{}^{11}B(OH)_3] \times [{}^{10}B(OH)_4^-]}{[{}^{10}B(OH)_3] \times [{}^{11}B(OH)_4^-]}. \quad (4)$$

Given a value for $^{11-10}K_B$ the isotopic composition of both boron species in seawater varies predictably with pH (Kakihana et al., 1977). The experimentally derived value 1.0272 ± 0.0006 in seawater at 25 °C is currently the preferred isotope fractionation factor (Klochko et al., 2006), which was previously also supported by theoretical studies (Zeebe, 2005). Providing $^{11-10}K_B$ and pK_B^*, the dissociation constant for boric acid at *in situ* temperature, salinity and pressure (commonly calculated according to Dickson, 1990), pH can be calculated from the $\delta^{11}B$ values of either boron species, e.g. borate ion:

$$pH = pK_B^* - \log\left[-\frac{\delta^{11}B_{sw} - \delta^{11}B_{borate}}{\delta^{11}B_{sw} - (^{11-10}K_B \times \delta^{11}B_{borate}) - 10^3 (^{11-10}K_B - 1)}\right] \quad (5)$$

where $\delta^{11}B_{sw}$ is the isotopic composition of seawater (39.61‰; Foster et al., 2010), consistent on timescales of 11 to 17 Ma due to the long residence time of boron in the ocean (Pagani et al., 2005; Paris et al., 2010; Lemarchand et al., 2012b).

Owing to the use of artificial culture medium (CM), the $\delta^{11}B_{sw}$ should be replaced by $\delta^{11}B_{CM}$, as its isotopic composition was different to that of natural seawater and was closely monitored during the full duration of the culturing. Although we observed a steady drift towards more isotopically depleted values over the culturing period (from approximately −3 to −6‰), at each given time the $\delta^{11}B_{CM}$ remained highly consistent (within the current analytical errors) in all culturing treatments (control and low-pH). Hence an exact comparison of the $\delta^{11}B$ of newly built shell material at the margin was possible between specimens cultured under different pH conditions (control pH_0 vs. and low-pH conditions pH_1 or pH_2). Following this approach we could precisely isolate the $\delta^{11}B$-pH response and establish a calibration for brachiopods. In order to make our culture calibration applicable to natural seawater conditions a simple normalisation was required. First, an adjustment of the $\delta^{11}B_{borate}$ in the cultures to $\delta^{11}B_{borate}$ of the natural seawater using the measured pH and $\delta^{11}B_{sw}$ (39.61‰) was required. Subsequently, the linear regression slopes of the culture calibrations (average y = 0.29x, Fig. 2) were fitted to the data of natural *M. venosa* (which are well constrained: $\delta^{11}B = 15.95‰$, see Section 2.4; $pH = 7.9 \pm 0.1$; see Section 2.1). This resulted in a single general calibration applicable to natural conditions (Fig. 3) without affecting

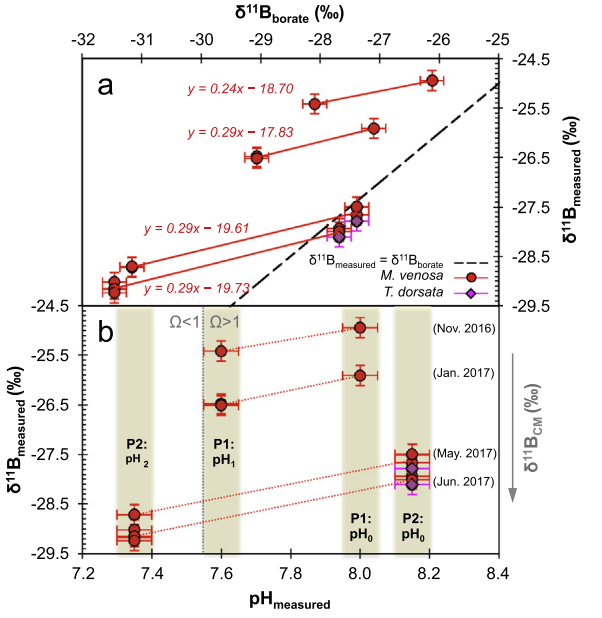

Fig. 2. Mini-bulk $\delta^{11}B$ (without normalisation) of shell parts grown under experimental conditions plotted in a: (a) $\delta^{11}B_{measured} - \delta^{11}B_{borate}$ space; and (b) $\delta^{11}B_{measured} - pH_{measured}$ space. The black line is the 1:1 relationship ($\delta^{11}B_{measured} = \delta^{11}B_{borate}$) following Klochko et al. (2006), red circles *M. venosa* data points (n = 16), purple rhombi *T. dorsata* (n = 2) data points. The $\delta^{11}B_{measured}$ is the measured $\delta^{11}B$ of brachiopod calcite, $\delta^{11}B_{borate}$ the pH-dependent composition of borate ion in the culture medium (CM), and $pH_{measured}$ the pH of CM. Each pair of data points connected with a trendline represents the $\delta^{11}B$ composition of a control and a low-pH sample at the same time, and thus at the same $\delta^{11}B_{CM}$. Due to a trend to more negative $\delta^{11}B_{cm}$ over the period of culturing (indicated by a grey arrow; see Section 2.6) an offset between the respective pairs exists. Yellow boxes highlight the culturing treatments, with time to which each data point corresponds approximated on the right side of panel b. (For interpretation of the references to colour in this figure legend, the reader is referred to the web version of this article.)

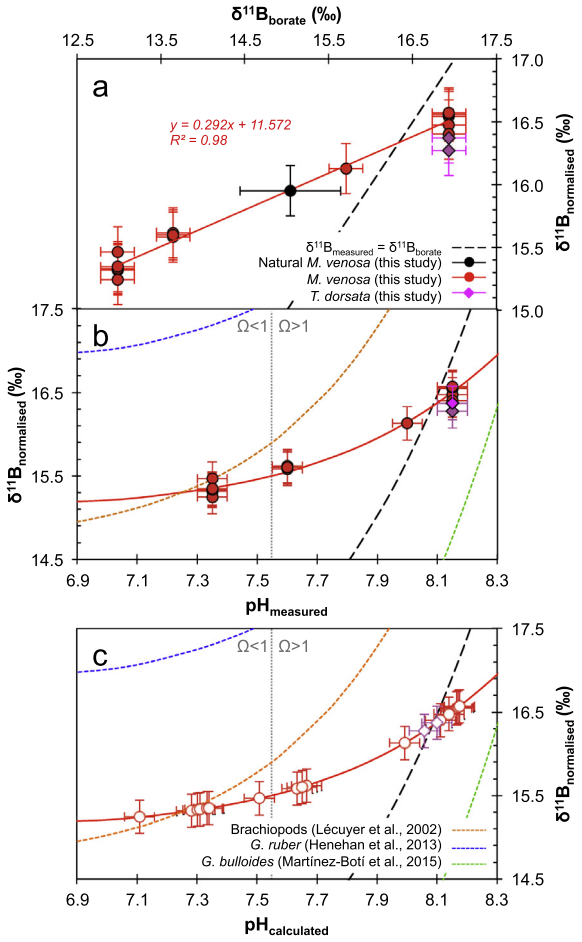

Fig. 3. Mini-bulk $\delta^{11}B$ results normalised to $\delta^{11}B_{sw} = 39.61‰$ (as described in Section 2.6); (a) new calibration for brachiopods plotted in a $\delta^{11}B_{measured} - \delta^{11}B_{borate}$ space. The black dashed line is the 1:1 relationship ($\delta^{11}B_{measured} = \delta^{11}B_{borate}$). The black circle shows the value for natural *M. venosa*. (b) Resulting $\delta^{11}B$–pH relationship for brachiopods, with the measured data points indicated. (c) Comparison between our $\delta^{11}B$–pH relationship and other curves from literature. The empty symbols indicate the calculated pH for our data points using the calibration presented in panel a. Here the black dashed line represents the aqueous $\delta^{11}B_{borate}$ values at given pH (Klochko et al., 2006); the coloured lines indicate relationships from other studies: a nature-based curve for biogenic carbonates including brachiopods (Lécuyer et al., 2002), a symbiont-bearing foraminifera *Globigerinoides ruber* (Henehan et al., 2013) and a symbiont-barren foraminifera *Globigerina bulloides* (Martínez-Botí et al., 2015) that envelope the typical spread as a result of varying degree of vital effects.

the slope and thus the sensitivity of *M. venosa* to pH. For all $\delta^{11}B$ to pH calculations we used $pK_B^* = 8.81$ (at temperature of 10 °C and salinity 30; Dickson, 1990). In contrast to the solution-based $\delta^{11}B$ data, the SIMS $\delta^{11}B$ data from cultured shell parts is presented without previously mentioned normalisation to natural seawater to allow a comparison between shell microstructures precipitated under natural and culture conditions. Thus shell material precipitated from natural $\delta^{11}B_{sw}$ bears a positive $\delta^{11}B$ signal, and from culture $\delta^{11}B_{CM}$ a markedly negative one ($\delta^{11}B < -20‰$). The B concentration in culture medium was comparable to natural seawater; around 0.5 mmol/l in contrast to 0.4 mmol/l measured for IAPSO.

2.7. Electron microprobe (EMP) analyses

JEOL JXA 8200 electron microprobe (EMP) mapping was used to assess elemental distribution and variations associated with shell microstructures. Quantitative elemental maps were obtained by wavelength dispersive x-ray spectrometry, simultaneously measuring Mg, Ca, Sr, Cl and S following Liebetrau et al. (2014) with modifications. In summary, the electron beam was focused to a spot size of 5 µm, accelerating voltage set to 15 kV and beam current to 100 nA. Mapping was repeated to gather 10 accumulations of the selected area at a step size of 5 µm and accumulation time of 15 ms, resulting in a resolution of 5 × 5 µm per pixel. Standard materials (Calcite, Sphalerite, Modern Coral-A2, Dolomite, KANI, Strontianite, VG-2, Scapolite) were measured before and after sample analyses to calculate absolute elemental concentrations, with uncertainties typically better than 2% relative standard deviation, 1σ).

2.8. Calcifying fluid pH measurements

Using H^+-selective microelectrodes we conducted *in vivo* pH measurements in the calcifying fluid. The H^+ microsensor construction and measurements were essentially performed as previously described in de Beer et al. (2008); Stumpp et al. (2012, 2013, 2015) and Ramesh et al. (2017). By plotting the voltage output of the probe against $\log[H^+]$ values, a linear regression yielded a Nernstian slope of >54 mV per 1 pH unit. With this method we were able to resolve a minimum difference of 0.1 pH units. For this, *M. venosa* from control (pH_0, n = 7) and low-pH (pH_2, n = 7) treatments were collected from the culturing tanks at GEOMAR and immediately transported to Kiel University in closed jars to minimise the gas exchange between culture medium and atmospheric air. Microelectrode measurements were performed within hours and once completed the brachiopods were returned to the cultures. The measurements were limited to juvenile individuals (<1 cm), which possess a transparent shell that enables manoeuvring of the microelectrode between the shell and the mantle epithelium. Measurements were performed under visual control of the sensor tip on an inverse microscope (Axiovert 135, Zeiss, Oberkochen, Germany) equipped with a temperature controlled water bath adjusted to 10 °C. Each sample was introduced into the measuring chamber containing 5 ml of seawater from the respective pH treatment. The ion-selective probe was mounted on a remote-controlled micromanipulator (Phytron) and introduced from the shell margin through the mantle into the calcifying fluid where the ionic activities were recorded.

3. RESULTS

3.1. Brachiopod growth in cultures

Experimental conditions of the different treatments are summarised in Table 1; the cultured species are shown in

Fig. 1. For *M. venosa* (Fig. 1a), we did not observe a difference in the growth of new shell material between the control ($pH_0 = 8.0$ and 8.15) and the low-pH treatments ($pH_1 = 7.6$ and $pH_2 = 7.35$) during either of the culturing phases. The typical growth rate of cultured *M. venosa* was about 1 mm per month, in line with observations made in nature (Baumgarten et al., 2013). Similarly, we noted that the growth rate was lower in larger individuals (>5 cm), possibly due to being close to reaching sexual maturity. The growth rate refers to simple measurements of the length of the shell valves (i.e. extension rate).

Information on *P. atlantica* regarding natural growth conditions is generally very limited and their growth rates are yet to be fully constrained (Álvarez et al., 2005; Logan, 2004). For the cultured organisms (Fig. 1c) it was not possible to distinguish any apparent new growth increments built during the culturing in either of the treatments by microscopic observations and calcein labelling. The only clue to their growth comes from SIMS $\delta^{11}B$ analyses, which enabled us to identify shell parts precipitated from natural seawater and from the culture medium because of the pronounced differences in the respective $\delta^{11}B$ (~40‰ vs. −3‰, respectively; see Section 2.6). By selective spot measurements we found microscopic regions in the anterior-most (youngest) part of the shell with negative $\delta^{11}B$ values down to minimum −20‰, implying that the area covered by the ion spot size corresponded to calcite almost entirely precipitated within the culture medium (Fig. 4a). Spots with more

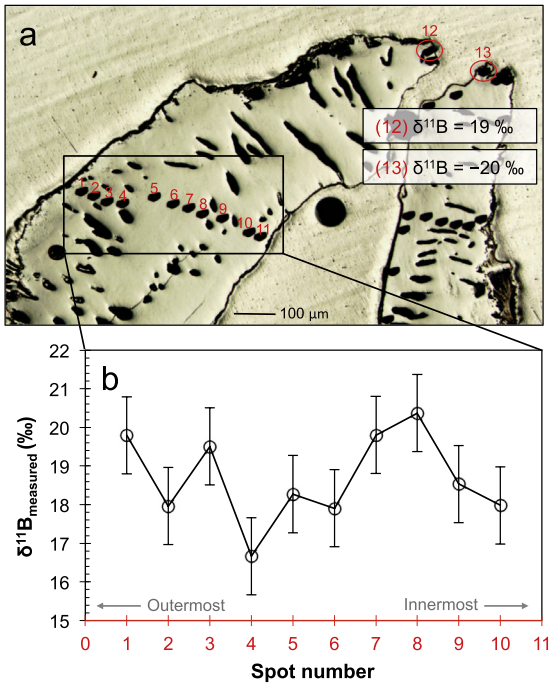

Fig. 4. Boron isotope measurements using secondary ion mass spectrometry (SIMS) in a cultured *P. atlantica* specimen; (a) microscope image showing the position of ion spots (numbered, in red) and the corresponding $\delta^{11}B$ values of the anterior-most (presumably youngest) dorsal and ventral valves; (b) $\delta^{11}B$ values for a profile across the dorsal valve, from outermost to innermost parts. (For interpretation of the references to colour in this figure legend, the reader is referred to the web version of this article.)

positive values, but lower than the $\delta^{11}B$ of natural *P. atlantica* ($\delta^{11}B = 19‰$), implied that the measured shell area contained material precipitated partially from natural seawater and partially from culture medium. In comparison, intrashell variations were rather small, potentially resulting from the different microstructures of the shell (Fig. 4b). This suggests a growth rate of less than 40 µm (the SIMS spot size) in 1.5 years. Whether this extremely slow growth rate may be an artefact of the artificial environment or is also true for natural organisms remains unclear, but if real could suggest surprisingly long lifespans of these organisms considering the average adult size of approximately 1 cm. As a consequence of the minimal growth in cultures, this species was not used for further $\delta^{11}B$ investigations.

3.2. Boron isotope calibration

Mini-bulk $\delta^{11}B$ data from *M. venosa* shell increments precipitated under specific pH conditions (as described in Section 2.3 and shown in Fig. 1) were used to establish a $\delta^{11}B$–pH calibration equation. The measured $\delta^{11}B$ values of our cultured brachiopods present a unique signature in contrast to natural brachiopods, because of the differences in our artificial $\delta^{11}B_{CM}$ and the natural $\delta^{11}B_{sw}$ (see Section 2.6). The initial $\delta^{11}B_{CM}$ at the start of experimental phase 1 (P1) was −3‰, with a progressive drift towards more depleted values throughout, resulting in −6‰ at the end of the experimental phase 2 (P2). The reason behind this progressive depletion of $\delta^{11}B_{CM}$ remains unclear, however we can exclude the successive refilling of evaporated volume by deionised water ($\delta^{11}B > 80‰$), as the boron background is expected to be heavy rather than light. Moreover, the B content of the deionised water source was regularly monitored (along with CM) on the ICP-OES and negligible (<0.005 mmol/l in deionised water against ~0.5 mmol/l in CM). This trend was highly consistent (within the current analytical errors) in all culturing treatments (control and acidification). By comparing the low-pH treatments to the respective controls we can isolate the $\delta^{11}B$-pH sensitivity for *M. venosa*. In Fig. 2 each pair of data points connected with a line represents the $\delta^{11}B$ composition of a control and a low-pH sample at a given time of culturing. The offset between these lines illustrates the slowly decreasing $\delta^{11}B_{CM}$ trend. All four calibration lines have highly consistent slopes (average $y = 0.29x$, Fig. 2), being controlled by the $\delta^{11}B$-pH sensitivity in *M. venosa*. By normalising the culture data to natural seawater and borate ($\delta^{11}B_{sw} = 39.61‰$, $\delta^{11}B$ of natural *M. venosa* = 16.0‰; see Section 2.6. for more details), we generate a universal calibration for conversion of natural brachiopod $\delta^{11}B_{calcite}$ to $\delta^{11}B_{borate}$ for pH-calculations (Fig. 3):

$$\delta^{11}B_{borate} = \frac{\delta^{11}B_{calcite} - (11.572 \pm 0.14)}{0.292 \pm 0.01} \quad (6)$$

The scatter in the data is minimal resulting in a close-fitting regression slope ($R^2 = 0.98$), and a clear response of $\delta^{11}B_{calcite}$ to the different $\delta^{11}B_{borate}$ (Fig. 3a). Eq. (6) is shown with standard errors for the slope and intercept, determined using the MS Excel function LINEST. In contrast to the aqueous borate ion $[B(OH)_4^-]$ to pH relationship

(dashed line), our brachiopod $\delta^{11}B$ data show a much shallower slope, plotting above the 1:1 line at the lower pH-end, and slightly below at the higher pH-end (Figs. 2a and 3a). While this calibration is predominantly based on *M. venosa* specimens, the sparse data available on *T. dorsata* from one treatment overlap within errors with the former. The resulting sensitivity to pH is shown in Fig. 3b. Although our curve confirms a clear $\delta^{11}B$–pH dependency for brachiopods, in comparison to the other relationships from the literature it records a rather diminished response to seawater pH changes. At present analytical uncertainties this suggests a limited proxy range to minimum pH of approximately 7.5, reconstructions below this value could potentially lead to large uncertainties due to the flattening of the $\delta^{11}B$–pH curve. For instance, a reverse pH reconstruction for a sample from the lowest pH treatment ($pH_2 = 7.35$) results in an apparent pH range within 7.1 and 7.5, entirely caused by the minimal analytical scatter on the order of below 0.2‰ (Fig. 3c).

3.3. Intrashell $\delta^{11}B$ variations

Prior to discussing our results we briefly review the terminology and structure of brachiopod shell for guidance (schematic diagram is available in Fig. 5). Brachiopod shell is secreted by epithelial cells of the mantle (Williams, 1966) in an accretionary growth mode (Ackerly, 1989). New increments are added to the shell margin as well as to the growth surface lining the mantle, resulting in a progressive elongation and thickening of the shell (Fig. 5). Accordingly, a multi-layered skeleton is developed composed of calcite increments secreted at different stages of life. Hence, the posterior part of the shell is dominated by an ontogenetic trend, while the anterior part of the shell consists of the youngest increment. At a microstructural level, the shell of terebratellid brachiopods including *M. venosa* is differentiated into two layers (although some species with an additional tertiary layer also exist): a thin (only few tenths of µm thick) outer primary layer of granular structure and a fibrous secondary layer (Fig. 6; see also e.g. Ye et al., 2018 for further details).

High spatial resolution data on $\delta^{11}B$ distribution within selected growth increments and shell layers are presented in Fig. 7. SIMS spots were arranged in vertical profiles that traverse the different calcification increments, which can be distinguished from Mg concentration EMP maps. High Mg content (in mostly green and yellow colours) is apparent on the edges of each successive increment and traces the growth lines produced under different ambient conditions: nature and the two experimental culturing phases (P1 and P2). The observed Mg 'banding' is present in shell parts grown under natural as well as culture conditions, indicating that this feature is not caused by seasonal variations. Since similar Mg patterns are obvious for both the control and the low-pH specimen the influence of pCO_2/pH changes on Mg distribution can also be excluded. Potentially, these Mg trends could be caused by growth related processes, which may lead to non-equilibrium effects during incorporation of Mg into the crystal lattice (Cusack et al., 2008). Increased Mg concentration is particularly apparent at the transition zones between the increments produced under different experimental conditions (indicated by arrows in Fig. 7), possibly as a result of short-term alteration of the precipitations rate due to stress from transport or calcein labelling.

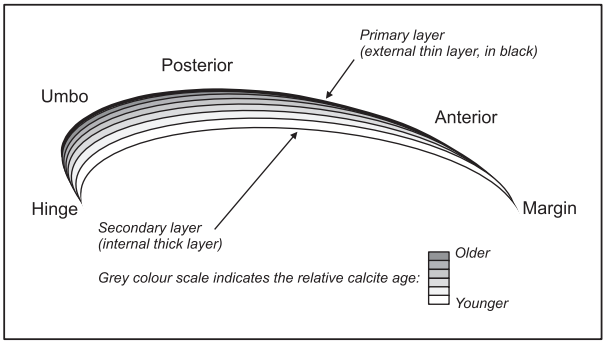

Fig. 5. Schematic diagram illustrating the accretionary growth of brachiopod shells (after Ackerly, 1989). Terminology used to refer to the different shell parts is also provided.

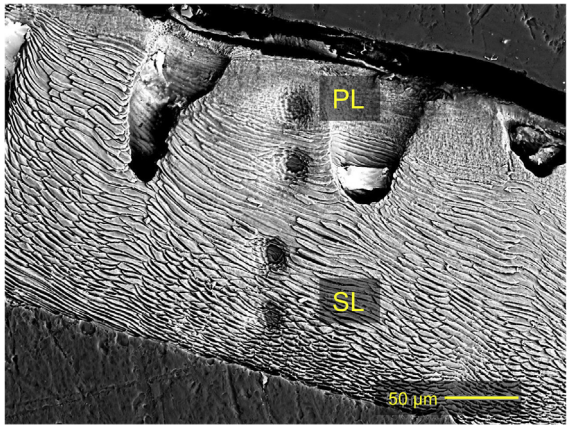

Fig. 6. Scanning electron microscope (SEM) image example depicting the different microstructures and a typical SIMS (secondary ion mass spectrometry) $\delta^{11}B$ profile. The image was taken after a weak acid leaching of the shell to remove the gold coating. Position of the ion spots is indicated – the upper spot is located in the outer primary layer (PL), the three lower spots are placed in the fibrous secondary layer (SL).

The SIMS profiles trace the $\delta^{11}B$ composition of the different increments and calcite layers from the outermost primary layer to the innermost secondary layer. An example of a typical SIMS profile within the shell microstructures is shown in the scanning electron microscope (SEM) image in Fig. 6. Based on an ontogenetic trend, the $\delta^{11}B$ profiles can be separated into anterior (Fig. 7: profiles a^3–a^5 and b^3–b^5) and posterior profiles (Fig. 7: profiles a^1–a^2 and b^1–b^2). While the anterior profiles are located in a recent shell increment formed entirely in the cultures, the posterior profiles cross the multiple shell increments precipitated at different stages of growth, including nature and culture conditions.

In the anterior part of the shell of the control specimen (Fig. 7a) the $\delta^{11}B$ decreases from isotopically heavier values

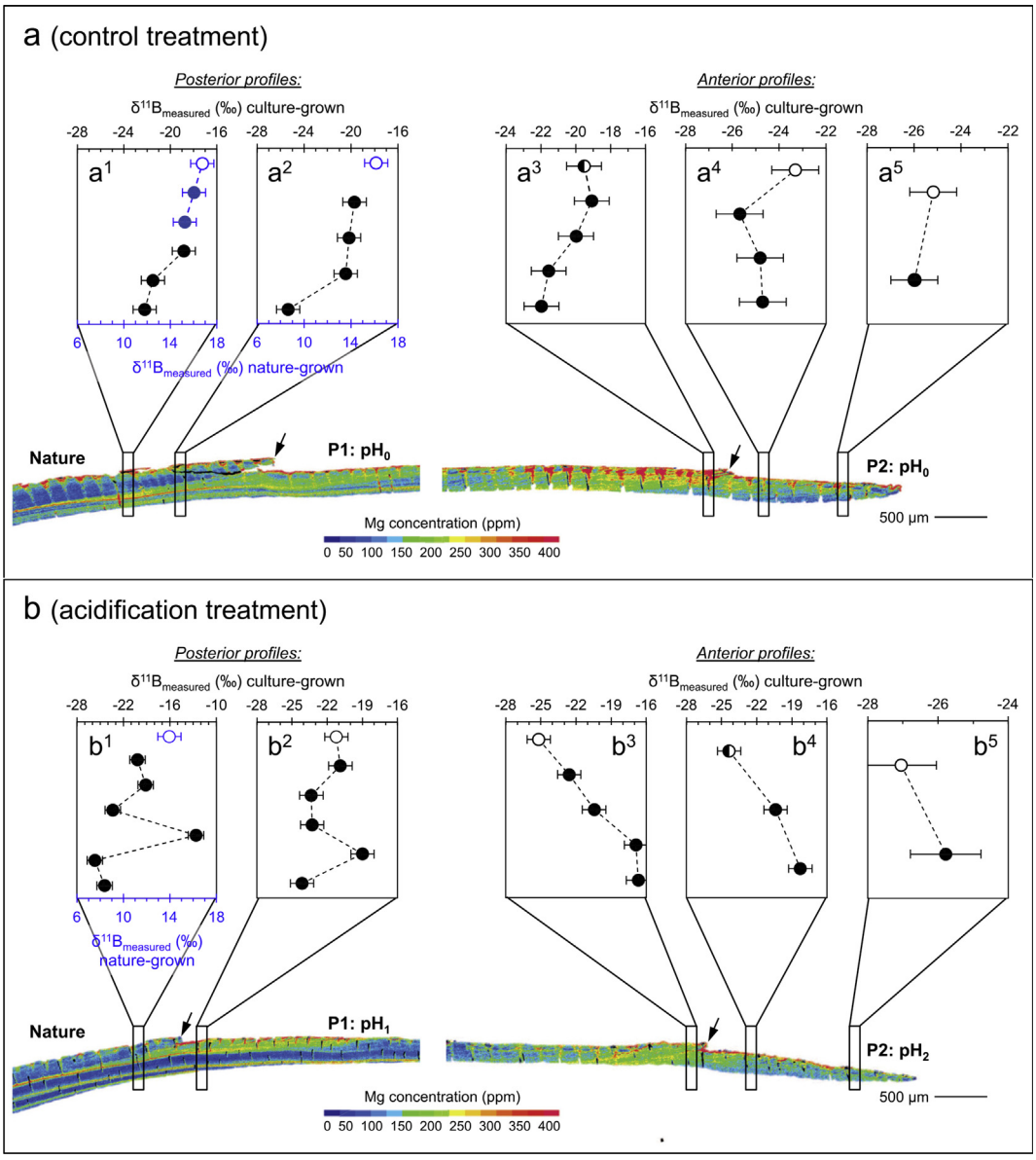

Fig. 7. Secondary ion mass spectrometry (SIMS) $\delta^{11}B$ profiles in cultured *M. venosa*: (a) cultured under control conditions (pH_0), and (b) low-pH conditions (pH_1 and pH_2). Position of the SIMS $\delta^{11}B$ profiles in the shells is shown in black boxes on the electron microprobe (EMP) Mg maps. Mg distribution maps highlights growth features, with elevated Mg content (in green) tracing specific shell increments. Outer protuberances (indicated by arrows) mark transition zones between increments formed in nature and the different experimental culturing phases P1 and P2. In the panels with $\delta^{11}B$ data (a^1–a^5 and b^1–b^5) black circles show measurements located in the shell parts grown purely under culturing conditions (negative $\delta^{11}B$ values, top x-axis); blue circles represent measurements located in shell parts grown in nature prior to culturing (positive $\delta^{11}B$ values, bottom x-axis). The pronounced difference between culture and nature $\delta^{11}B$ of the shell is due to precipitation from solution of different $\delta^{11}B$; $\delta^{11}B_{CM}$ vs. $\delta^{11}B_{sw}$ (see Section 2.6 for more details). Filled symbols illustrate measurements located entirely in the secondary layer, empty symbols in the primary layer, and half-filled show the spots with significant contribution of both layers.

in the outermost primary layer to lighter values in the innermost secondary layer (Fig. 7a: profiles a^3–a^5). In the low-pH specimen (Fig. 7b), the trend is opposite; the primary layer is relatively light while the secondary layer is more enriched in the heavy isotopes (Fig. 7b: profiles b^3–b^5). In contrast to the anterior shell margin, the posterior area is composed of multiple layers in both specimens (control and low-pH) as indicated by the EMP Mg maps, which results in more complex $\delta^{11}B$ profiles (Fig. 7: profiles a^1–a^2 and b^1–b^2). The $\delta^{11}B$ of the upper increments (older) precipitated under natural conditions (before culturing) is typically positive (about 16‰), whereas underneath the inner increments bear a negative $\delta^{11}B$ signal indicating that they were formed within the culture medium.

3.4. Calcifying fluid pH

Microelectrode measurements of pH in the calcifying fluid between the shell and the mantle tissue (Fig. 8a and b) were carried out to evaluate the internal pH-regulatory capacity of *M. venosa*. Our results are summarised in Fig. 8c, and indicate a relatively narrow pH range in the calcifying fluid, with a median around ~7.8 (Fig. 8c) for individuals cultured under control ($pH_0 = 8.15$) as well as low-pH ($pH_2 = 7.35$) conditions. The box plots are based on measurements in seven brachiopods from each treatment and thus reflect the variance within individuals. We note that these measurements were performed outside of the culturing tanks, and thus a slight offset (~0.1 pH units) in the pH of the CM measured in culturing facilities (as given in Table 1) and under the microscope setup using microelectrodes (particularly at low-pH) was observed due to CO_2 degassing and different ambient conditions.

4. DISCUSSION

4.1. Boron isotope composition of brachiopods

Brachiopods have been considered faithful $\delta^{11}B$ recorders, as their composition apparently reflects the seawater borate ion. Measurements of natural samples have shown that $\delta^{11}B$ values of modern samples are within the range of foraminifers and thus could be used for palaeoreconstructions (Lécuyer et al., 2002). Leaving the culturing experiments aside for now, our measured $\delta^{11}B$ of natural *M. venosa* and *P. atlantica* samples already indicate the feasibility of the $\delta^{11}B$–pH proxy in brachiopods (Table 2). For instance, at pH of 8 and $\delta^{11}B_{sw}$ ~39.6‰, the $\delta^{11}B_{borate}$ is expected to be ~15.7‰. Providing that only borate ion is incorporated into brachiopods, as largely expected for biogenic carbonates (e.g. Hemming and Hanson, 1992), the $\delta^{11}B$ of brachiopod shells should mimic the seawater borate. Our measurements of natural *M. venosa* give a $\delta^{11}B$ ~16.0‰, which agrees very well with the expected borate ion values (~15.7‰). A similar exercise can be applied to *P. atlantica*, using the pH and ambient conditions as provided in Table 2, the $\delta^{11}B_{borate}$ of local seawater is expected to be ~19.1‰ while the *P. atlantica* give a $\delta^{11}B$ ~18.9‰, highly consistent within the uncertainties. Moreover, both species are morphologically very different, possess distinct biomineralisation mechanisms and have contrasting growth rates. This supports the notion that only borate ion appears to be incorporated into brachiopod calcite. Potentially, it could also indicate that inter-specific differences are not too large and do not obscure the seawater $\delta^{11}B_{borate}$, but this needs further confirmation with other modern species. We note, however, that for a definite eval-

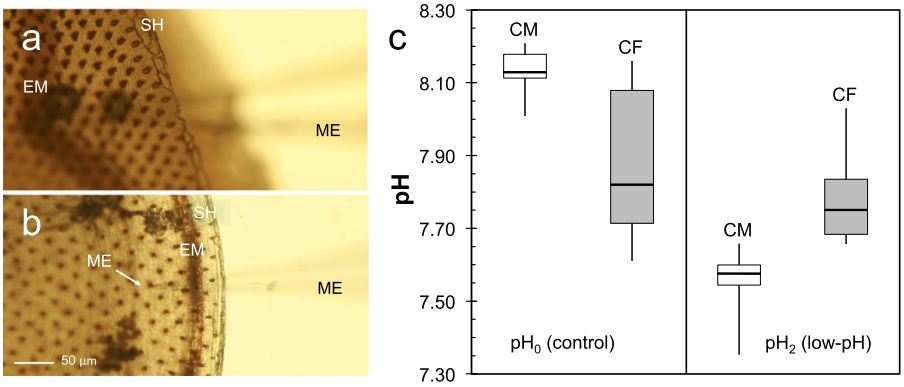

Fig. 8. Microelectrode pH measurements in the calcifying fluid. Left panels: photographs taken from below of the *M. venosa* specimen (anterior part of the valve) through an inverted microscope; (a) the electrode is pressed into the mantle; (b) the electrode perforated the mantle and is in measurement position between the shell and the epithelium. SH–shell (outside), EM–epithelial mantle, ME–microelectrode (V-shaped contour). Right panel: (c) Measured pH_{NBS} of seawater (SW) and calcifying fluid (CF) in pH_0 (control) and pH_2 (low-pH) treatments. The minimum and maximum values are indicated by the whiskers, lower and upper boxes show the third and first quartiles, respectively with a thicker median line between them (n = 7 for each box plot). (For interpretation of the references to colour in this figure legend, the reader is referred to the web version of this article.)

Table 2
Boron isotope composition of the natural brachiopod samples (not cultured), including mean annual temperature, salinity and pH of in the local environment.

Species	Location	Sal.	T. [°C]	pH	$\delta^{11}B$ [‰]
Magellania venosa	Comau Fjord, Chile	30	10	7.9	15.95
Pajaudina atlantica	La Palma, Canary Islands	36	21	8.1	18.86

uation a good knowledge on seawater pH is critical, which is not straightforward in nature. Ultimately, it will be difficult to convincingly rule out presence of boric acid in the calcite until these measurements are attempted, but at present all points towards borate ion being the only species incorporated into brachiopod shells.

4.2. Effect of acidification on brachiopods

Reduced skeletal growth due to CO_2-induced ocean acidification and associated changes in calcium carbonate saturation state of seawater (Ω_{cal}) has been well documented in a broad range of marine organisms including corals, molluscs, foraminifera, coccolithophores, or coralline algae (e.g. Gazeau et al., 2007; Fabry et al., 2008; Silverman et al., 2009; Ries et al., 2009; Kroeker et al., 2013), yet only little is known on the effect on brachiopods. During our experiments, all cultured brachiopods survived without obviously affected growth prolonged acidification such as that predicted for the end-century surface ocean ($pH_1 = 7.6$; Table 1; e.g. Brewer, 1997), or even much more extreme conditions involving further reduction of seawater pH ($pH_2 = 7.35$) and calcite saturation state ($\Omega_{cal} = 0.6$). This points to a strong biological control on the shell formation and the internal pH of *M. venosa*. Potentially, similar controlling mechanism may also be present in *T. dorsata*, and *P. atlantica*, although this could not be fully evaluated by the present study due to the lack of individuals of the first species, and elusive growth of the second. Unaffected survival and shell building under acidification has also been reported for the Antarctic brachiopod *Liothyrella uva* (Cross et al., 2015) and the New Zealand *Calloria inconspicua* (Cross et al., 2016). It appears that several brachiopod species, and especially terebratellids, may not be negatively affected by regimes with reduced pH, or at least the effect of low-pH alone. Experiments combining acidification with additional stressors such as temperature increase or nutrient limitation indicate that it is the synergic effect of stressors that is particularly detrimental to physiological processes of calcifying organisms (e.g. Reynaud et al., 2003; Holcomb et al., 2010). These experiments present a more representative scenario for natural systems under increasing anthropogenic pressures, and thus it remains highly questionable whether brachiopods will be able to accommodate to these changes despite the apparent robust pH-buffering capacities.

4.3. Vital effects

The survival and calcification of *M. venosa* under acidified conditions and at thermodynamically unfavourable conditions with respect to calcite precipitation ($\Omega_{cal} < 1$), point towards a strong biological control over shell growth. This is also evident from the shallow slope of our brachiopod boron isotope fractionation line in comparison to the expected aqueous $\delta^{11}B_{borate}$ composition (Fig. 2a and a), and the resulting moderate response of $\delta^{11}B_{calcite}$ to pH changes (Fig. 3b and c). The calibration crosses the 1:1 line (where $\delta^{11}B_{measured}$ = aqueous $\delta^{11}B_{borate}$) recording similar $\delta^{11}B_{calcite}$ than that of aqueous $\delta^{11}B_{borate}$ at normal culture medium pH, but higher $\delta^{11}B_{calcite}$ at acidified conditions (Fig. 3a). This suggests a reduced pH range at precipitation, which is likely caused by regulation of their calcifying fluid. To determine whether internal physiological pH-buffering may be responsible for the observed trend we performed *in vivo* calcifying fluid measurements at the interface of the epithelial mantle and the shell as shown in Fig. 8 on several *M. venosa* individuals from control (pH_0) and low-pH (pH_2) treatments. The calcite formation is anticipated to occur at the mantle-shell interface via ion-transporting channels in a fluid-filled medium – which is here referred to as the calcifying fluid – of μm to sub-μm dimensions. Our results indicate a rather narrow pH range in the calcifying fluid (~7.8; Fig. 8c), below normal seawater conditions, which does not appear to be affected by the pH of the culture medium, or at least could not be resolved considering the variance in the date. Although these measurements were performed on juvenile organisms (<1 cm), we do not expect the pH to differ significantly in the typical adults (2–5 cm), since the growth rates of *M. venosa* are relatively constant over the different life stages (with the exception of the oldest organisms >5 cm that have lower growth rates; Baumgarten et al., 2013). This demonstrates that *M. venosa* are able to strictly control their calcifying fluid pH, leading to stable pH conditions at the calcification front even in an environment with low-pH conditions. Similar phenomenon has also been reported for corals (Georgiou et al., 2015; Wall et al., 2015), and our study now confirms it for brachiopods.

What remains to be answered is why would brachiopods calcify at such low-pH, when compared to most of the other calcifiers. For instance, the cold-water coral *Desmophyllum dianthus* from the same habitat as *M. venosa* in Chile has a calcifying fluid pH of ~8.7 (McCulloch et al., 2012b), much higher than seawater. Since brachiopods are an evolutionary old taxon (earliest known brachiopods occur in the lowermost Cambrian, Holmer and Popov, 1996) it could be that their calcification mechanisms differ from many other calcifiers and potentially bear a link to ancient seawater chemistry. Seawater pH estimates for the early Phanerozoic predict values as low as ~7.4 (Halevy and Bachan, 2017). Early ancestors would have to accommodate to these environmental conditions, and calcification pathways requiring substantial up-regulation of calcifying fluid pH with respect to seawater would not pose a physiologically efficient mechanism. The problem of low seawater pH can be overcomed if the preferred substrate for calcification is bicarbonate, and not carbonate, which is also the dominant DIC species at the respective pH. Relevant enzymatic systems such as carbonic anhydrases catalyse the reversible hydration of carbon dioxide into bicarbonate and free protons: $CO_2 + H_2O \leftrightarrow HCO_3^- + H^+$ and could present a highly effective mechanism for calcification under low-pH/high-DIC conditions (Moya et al., 2008; Bertucci et al. 2009; Khalifah, 1971). This could explain the ability of *M. venosa* and as well as other terebratellids to thrive in low-pH environments without hampered shell growth.

In summary, we identify vital effects on $\delta^{11}B$ in brachiopods as internal pH-regulation. Taking into account the reduced $\delta^{11}B$–pH sensitivity (Fig. 3), it is apparent that the mini-bulk $\delta^{11}B$ composition of the shell, integrates to a

certain (and potentially large) extent the calcifying fluid pH. The distortion of the ambient pH signal (deviation from the aqueous $\delta^{11}B_{borate}$) thus seems to be primarily caused by homeostasis. Further work and especially refining the uncertainties of the calcifying fluid measurements is required for a more conclusive evidence, but if true it would mean that $\delta^{11}B$ in brachiopods fully reflects the pH of solution from which it precipitated. This would imply that incorporation of boron into brachiopod calcite follows the inorganic fractionation relationship (Klochko et al., 2006), and that no boric acid is co-precipitated, which is rather unexpected for a calcitic matrix (e.g. Noireaux et al., 2015).

4.4. Boron isotope composition of shell microstructures

Above we directly and indirectly demonstrate that brachiopods regulate their calcifying fluid pH, which appears to be to a certain extent probed by the (mini-bulk) $\delta^{11}B$. Still, despite the confined calcification pH range, a $\delta^{11}B$–pH dependency exists. This raises a question on the underlying basis of the $\delta^{11}B$–pH dependency, which could be caused by two potential mechanisms. The first possibility would be that the brachiopod calcifying fluid is systematically impacted by ocean acidification, as apparently true for corals (Hönisch et al., 2004; Reynaud et al., 2004; Krief et al., 2010; Venn et al., 2013; Gagnon, 2013; Wall et al., 2016; Stewart et al., 2016), but the effect is relatively minor and could not be resolved by our calcifying fluid pH measurements. An alternative or additional option would be that the ambient seawater pH signal is, at least partially, attained in specific parts of the calcite (in this case shell layers), and cannot be detected via mini-bulk or bulk approaches. To reconcile the interpretation of the (mini-bulk) $\delta^{11}B$ data we examine the $\delta^{11}B$ composition of *M. venosa* shell microstructures from SIMS measurements (Fig. 7). Description of the brachiopod shell structure is provided in Section 3.3. Particularly relevant are also Figs. 5 and 6, which illustrate the shell features discussed in this section.

The shell of *M. venosa* is composed of two calcite layers with different microstructures: an outer primary layer of granular structure and a fibrous secondary layer (Fig. 7). Differences in boron and other isotope system compositions of the two layers have been documented, attributed to distinct biomineralisation processes during the formation of the layers. In brachiopods from natural settings, a shared trend was observed where the primary layer was isotopically lighter in contrast to the secondary layer, which was closer to equilibrium with seawater (Penman et al., 2013; Cusack et al., 2012; Bajnai et al., 2018; Romanin et al., 2018). Strikingly, this is not apparent in the cultured brachiopods and our results indicate that the respective direction of the trend principally depends on the ambient seawater pH. Progressive depletion in $\delta^{11}B$ from the outermost primary layer to the innermost secondary layer in the control specimen (Fig. 7a: profiles a^3–a^5) and enrichment in the low-pH specimen (Fig. 7b: profiles b^3–b^5) indicate that biomineralisation differences between the primary and the secondary layer do not seem to significantly affect the $\delta^{11}B$. Instead, the intrashell variations may be explained by a physiological gradient produced by an interplay of two end members of different pH, the calcifying fluid and the seawater, the first driving the $\delta^{11}B$ composition of the innermost and the latter of the outermost layer. This would imply that kinetic effects resulting from the different biomineralisation modes between primary and secondary layer do not significantly affect $\delta^{11}B$ values, or at least cannot be resolved with the present analytical error of SIMS. This is also in line with what is expected for the boron isotope system, considering the relative slow growth of brachiopods and the fast equilibration of boric acid with borate ion (~125 μs; Zeebe et al., 2001). More recently, however, precipitation experiments using synthetic calcite found growth rate effects on boron mineral-fluid partitioning and fractionation (Gabitov et al., 2014; Mavromatis et al., 2015; Uchikawa et al., 2015; Kaczmarek et al., 2016). Comparisons between purely inorganic system and any biogenic calcite are however not straightforward because of the different nature of the systems as well as disparate growth rates involved. While the exact role of kinetic effects on $\delta^{11}B$ in biogenic carbonates still remains an open question, our results indicate that it is not the dominant factor behind the intrashell $\delta^{11}B$ variations in brachiopods.

In the posterior region, where the shell structure is dominated by an ontogenetic trend the $\delta^{11}B$ profiles enable us to trace the calcite sheets precipitated from solutions of different $\delta^{11}B$ composition – $\delta^{11}B_{CM}$ vs. $\delta^{11}B_{sw}$ (Fig. 7: profiles a^1–a^2, b^1–b^2). Together with the Mg distribution maps, this permits us to identify the origin of each of the shell increments and illustrates the accretionary growth mechanism. The oldest shell part precipitated from natural seawater forms the outermost layer and has a composition of ~16‰ (Fig. 7: profiles a^1–a^2 and b^1, shown in blue symbols). Below, the intermediate shell layer was formed at the onset of the culturing experiments and was built from initial $\delta^{11}B_{CM}$ (~−3‰). The final increment is the youngest and has the lightest $\delta^{11}B$ values, implying that it was built towards the end of the culturing experiments from most depleted $\delta^{11}B_{CM}$ (~−6‰). A particularly interesting feature of these profiles are the $\delta^{11}B$ values of about −13‰ measured in the acidification specimen (Fig. 7b: profiles b^1–b^2). This composition may only be achieved by mixing of both, nature and culture grown components, yet the −13‰ values were measured in an increment built entirely under culture conditions. Terebratellids have been found to possess robust repair processes (Cross et al., 2015, 2016), which could explain the observed value, providing that mobilisation of older material was also involved.

5. CONCLUSIONS

This study provides novel direct and indirect evidences on the internal pH-controlling mechanisms of the brachiopod *M. venosa*, which potentially may also be relevant for other brachiopod species, in particular *T. dorsata* or other terebratellids. *M. venosa* regulate their calcifying fluid pH, which is maintained at a narrow pH range below normal seawater pH, suggesting the use of bicarbonate ion as the preferred calcification substrate. This physiological

adaptation makes these calcifiers resilient to CO_2-driven ocean acidification and explains their ability to survive in low-pH conditions, even at $\Omega_{cal} < 1$ without hampered shell growth. Presumably, this mechanism developed early during metazoan evolution and played an important role in determining brachiopod survival through the multiple Phanerozoic environmental crises. We establish a $\delta^{11}B$–pH relationship for brachiopods, which supports their application as an archive for palaeo-pH and palaeo-CO_2 reconstructions. Our culture-based calibration, however, shows a more attenuated $\delta^{11}B$–pH response than previously thought due to the strong role of biological processes over shell formation. This results in a reduced dynamic proxy range for brachiopods, demanding caution as small $\delta^{11}B$ variations in the calcite matrix would lead to potentially large differences in the calculated pH values, particularly at very low-pH conditions. In contrast to the clear pH-dependency confirmed by mini-bulk data, at a micro-scale level we observe marked $\delta^{11}B$ intra-shell heterogeneities. While an ontogenetic trend certainly plays an important role, at present it appears that $\delta^{11}B$ variations between the outermost and the innermost layers may be explained in context of a physiological gradient across the shell. Accordingly, boron incorporation into the innermost shell layers is primarily driven by calcifying fluid pH, whereas the outermost calcite layers are to some extent influenced by ambient seawater pH. Increased analytical precision is needed before a conclusive statement can be made, but if true, this may suggest rather unexpected $\delta^{11}B$ fractionation for a biogenic calcite. In addition, this could offer an explanation for the basis behind the mini-bulk $\delta^{11}B$–pH dependency, although it is also possible that calcifying fluid pH is systematically impacted by ocean acidification, which could contribute to the $\delta^{11}B$–pH trend. Finally, we would like to encourage further research on brachiopods involving controlled culturing experiments under both, laboratory and/or mesocosm conditions, which clearly proves invaluable for advancing our understanding on the geochemistry, biology as well as physiological adaptations of these marine calcifiers to cope with environmental change.

ACKNOWLEDGMENTS

We thank the staff of Huinay Scientific Field Station for logistical support on our scientific dive expeditions to collect *M. venosa* and *T. dorsata*. For assistance during sampling of *P. atlantica* we acknowledge Alex Neubert, Georg Maghon and Barbara Wolters from Tauchpartner, La Palma. We are grateful to Finn-Ole Petersen for help with the culturing, Ana Kolevica, Inga Viebrock and Tyler Goepfert for laboratory support, Regina Surberg for ICP-OES measurements, Mario Thöner for assistance with electron microprobe analyses, and Nordine Bouden for technical help on the ion microprobe. This project has received funding from the European Union's Horizon 2020 research and innovation programme under the Marie Sklodowska-Curie grant agreement No. 643084 (BASE-LiNE Earth), and was also supported by the collaborative research initiative CHARON (DFG Forschergruppe 1644- Phase II) funded by the German Research Foundation (DFG). M.Y.H. was funded by the DFG Emmy Noether Programme HU 2611/1-1. This manuscript benefited from constructive suggestions of Claire Ross, two anonymous reviewers, and the associate editor James Farquhar.

REFERENCES

Ackerly S. C. (1989) Kinematics of accretionary shell growth, with examples from brachiopods and molluscs. *Paleobiology* **15**, 147–164.

Aggarwal S. K. and You C.-F. (2016) A review on the determination of isotope ratios of boron with mass spectrometry. *Mass Spectrom. Rev.* **9999**, 1–21.

Al-Horani F. A., Al-Moghrabi S. M. and de Beer D. (2003) The mechanism of calcification and its relation to photosynthesis and respiration in the scleractinian coral *Galaxea fascicularis*. *Mar. Biol.* **142**, 419–426.

Anagnostou E., Huang K. F., You C. F., Sikes E. L. and Sherrell R. M. (2012) Evaluation of boron isotope ratio as a pH proxy in the deep sea coral *Desmophyllum dianthus*: evidence of physiological pH adjustment. *Earth Planet. Sci. Lett.* **349**, 251–260. https://doi.org/10.1016/j.epsl.2012.07.006.

Atkinson M. J. and Bingman C. (1998) Elemental composition of commercial seasalts. *J. Aquaricult. Aquat. Sci.* **7**, 39–43.

Álvarez F., Martínez A., Núñez L. and Núñez J. (2005) Sobre la presencia en Canarias de varias especies de braquiópodos (Brachiopoda: Rhynchonellata) en cuevas y cornisas submarinas. *Vieraea* **33**, 261–279.

Bajnai D., Fiebig J., Tomašovych A., Milner García S., Rollion-Bard C., Raddatz J., Löffler N., Primo-Ramos C. and Brand U. (2018) Assessing kinetic fractionation in brachiopod calcite using clumped isotopes. *Sci. Rep.* **8**, 533.

Balan E., Noireaux J., Mavromatis V., Saldi G. D., Montouillout V., Blanchard M., Pietrucci F., Gervais C., Rustad J. R., Schott J. and Gaillardet J. (2018) Theoretical isotopic fractionation between structural boron in carbonates and aqueous boric acid and borate ion. *Geochim. Cosmochim. Acta* **222**, 117–129.

Barker S., Greaves M. and Elderfield H. (2003) A study of cleaning procedures used for foraminiferal Mg/Ca paleothermometry. *Geochem. Geophys. Geosyst.* **4**(9), 8407. https://doi.org/10.1029/2003GC000559.

Baumgarten L. J., McLellan M., Robinson W., Forbes J., McGuffie P., Jess L. and Malcolm B. (2012) The influences of saline concentration on the success of Calcein marking techniques for hatchery-produces Murray cod (*Maccullochella peelii*). *J. Proc. R. Soc. N.S.W.* **145**, 168–180.

Baumgarten S., Laudien J., Jantzen C., Häussermann V. and Försterra G. (2013) Population structure, growth and production of a recent brachiopod from the Chilean fjord region. *Mar. Ecol.* **35**, 401–413.

Bertucci A., Innocenti A., Zoccola D., Scozzafava A., Allemand D., Tambutté S. and Supuran C. T. (2009) Carbonic anhydrase inhibitors: inhibition studies of coral secretory isoform with inorganic anions. *Bioorg. Med. Chem. Lett.* **19**, 650–653.

Blamart D., Rollion-Bard C., Meibom A., Cuif J.-P., Juillet-Leclerc A. and Dauphin Y. (2007) Correlation of boron isotopic composition with ultrastructure in the deep-sea coral *Lophelia pertusa*: Implications for biomineralisation and paleo-pH. *Geochem. Geophys. Geosyst.* **8**. https://doi.org/10.1029/2007GC001686.

Brand U. and Veizer J. (1980) Chemical diagenesis of multicomponent carbonate system-1: trace elements. *J. Sediment. Petrol.* **50**, 1219–1236.

Brand U. and Veizer J. (1981) Chemical diagenesis of multicomponent carbonate system-2: stable isotopes. *J. Sediment. Petrol.* **51**, 987–997.

Brand U., Logan A., Hiller N. and Richardson J. (2003) Geochemistry of modern brachiopods: applications and implications for oceanography and paleoceanography. *Chem. Geol.* **198**, 305–334. https://doi.org/10.1016/S0009-2541(03)00032-9.

Brand U., Posenato R., Came R., Affek H., Angiolini L., Azmy K. and Farabegoli E. (2012) The end-Permian mass extinction: a rapid volcanic CO_2 and CH_4-climatic catastrophe. *Chem. Geol.* **323**, 121–144. https://doi.org/10.1016/j.chemgeo.2012.06.015.

Brewer P. G. (1997) Ocean chemistry of the fossil fuel CO_2 signal: the haline signal of "business as usual". *Geophys. Res. Lett.* **24**, 1367–1369.

Carlson S. J. (2016) The evolution of brachiopoda. *Annu. Rev. Earth Planet. Sci.* **44**, 409–438.

Cross E. L., Peck L. S. and Harper E. M. (2015) Ocean acidification does not impact shell growth or repair of the Antarctic brachiopod *Liothyrella uva* (Broderip, 1833). *J. Exp. Mar. Biol. Ecol.* **462**, 29–35.

Cross E. L., Peck L. S., Lamare M. D. and Harper E. M. (2016) No ocean acidification effects on the shell growth and repair in the New Zealand brachiopod *Calloria inconspicua* (Sowerby, 1846). *J. Mar. Sci.* **73**, 920–926. https://doi.org/10.1093/icesjms/fsv031.

Catanzaro E. J., Champion C. E., Garner E. L., Marinenko G., Sappenfield K. M. and Shields W. R. (1970). In *Standard Reference Materials: Boric acid; Isotopic and Assay Standard Reference Materials. US National Bureau of Standards, Special Publication*, pp. 260–317.

Cusack M., Pérez-Huerta A., Janousch M. and Finch A. A. (2008) Magnesium in the lattice of calcite-shelled brachiopods. *Chem. Geol.* **257**, 59–64.

Cusack M., Pérez-Huerta A. and EIMF (2012) Brachiopods recording seawater temperature – a matter of class of maturation? *Chem. Geol.* **334**, 139–143.

de Beer D., Bisset A., de Wit R., Jonkers H., Köhler-Rink S., Nam H., Kim B. H., Eickert G. and Grinstain M. (2008) A microsensor for carbonate ions suitable for microprofiling in freshwater and saline environments. *Limnol. Oceanogr. Methods* **6**, 532–541.

de Nooijer L. J., Toyofuku T. and Kitazato H. (2009) Foraminifera promote calcification by elevating their intracellular pH. *Proc. Natl. Acad. Sci.* **106**, 15374–15378.

Dickson A. G. (1990) Thermodynamics of the dissociation of boric-acid in synthetic seawater from 273.15-k to 318.15-k. *Deep-Sea Res. A, Oceanorg. Res. Pap.* **37**, 755–766. https://doi.org/10.1016/0198-0149(90)90004- F.

Fabry V. J., Seibel B. A., Feely R. A. and Orr J. C. (2008) Impacts of ocean acidification on marine fauna and ecosystem processes. *ICES J. Mar. Sci.* **65**, 414–432.

Farkaš J., Böhm F., Wallmann K., Blenkinsop J., Eisenhauer A., van Geldern R., Munecke A., Voigt S. and Veizer J. (2007) Calcium isotope record of Phanerozoic oceans: implications for chemical evolution of seawater and its causative mechanisms. *Geochim. Cosmochim. Acta* **71**, 5117–5134.

Fietzek P., Fiedler B., Steinhoff T. and Körtzinger A. (2014) In situ quality assessment of a novel underwater pCO_2 sensor based on membrane equilibration and NDIR spectrometry. *J. Atmos. Oceanic Technol.* **31**, 181–196.

Foster G. L. (2008) Seawater pH, pCO_2 and $[CO_3^{2-}]$ variations in the Caribbean Sea over the last 130 kyr: a boron isotope and B/Ca study of planktic foraminifera. *Earth Planet. Sci. Lett.* **271**, 254–266. https://doi.org/10.1016/j.epsl.2008.04.015.

Foster G. L., Pogge von Strandmann P. A. E. and Rae J. W. B. (2010) Boron and magnesium isotopic composition of seawater. *Geochem. Geophys. Geosyst.* **11**, Q08015. https://doi.org/10.1029/2010GC003201.

Gabitov R. I., Rollion-Bard C., Tripati A. and Sadekov A. (2014) *In situ* study of boron partitioning between calcite and fluid at different crystal growth rates. *Geochim. Cosmochim. Acta* **137**, 81–92.

Gagnon A. C. (2013) Coral calcification feels the acid. *Proc. Natl. Acad. Sci.* **110**, 1567–1568.

Garbelli C., Angiolini L. and Shen S.-Z. (2017) Biomineralization and global change: a new perspective for understanding the end-Permian extinction. *Geology* **45**, 19–22.

Gazeau F., Quiblier C., Jansen J. M., Gattuso J.-P., Middelburg J. J. and Heip C. H. R. (2007) Impact of elevated CO_2 on shellfish calcification. *Geophys. Res. Lett.* **34**, L07603. https://doi.org/10.1029/2006GL028554.

Georgiou L., Falter J., Trotter J., Kline D. I., Holcomb M., Dove S. G., Hoegh-Guldberg O. H. and McCulloch M. (2015) pH homeostasis during coral calcification in a free ocean CO_2 enrichment (FOCE) experiment, Heron Island reef flat, Great Barrier Reef. *Proc. Natl. Acad. Sci.* **112**, 13219–13224.

Guimerans P. V. and Cañavate A. R. (1994) *Oceanographic Characteristics of the Canary Islands Waters*. International Hydrographic Review, Monaco, LXXI(l).

Gutjahr M., Ridgewell A., Sexton P. F., Anagnostou E., Pearson P. N., Pälike H., Norris R. D., Thomas E. and Foster G. L. (2017) Very larger release of mostly volcanic carbon during the Palaeocene-Eocene Thermal Maximum. *Nature* **548**, 573–577.

Halevy I. and Bachan A. (2017) The geologic history of seawater pH. *Science* **355**, 1069–1071.

Häussermann V. and Försterra G. (2009) *Marine Benthic Fauna of Chilean Patagonia*. Nature in Focus, Puerto Montt, p. 1000.

Henehan M. J., Rae W. B., Foster G. L., Erez J., Prentice K. C., Kucera M., Bostock H. C., Martínez-Botí M. A., Milton J. A., Wilson P. A., Marshall B. J. and Elliott T. (2013) Calibration of boron isotope proxy in the planktonic foraminifera *Globigerinoides ruber* for use in palaeo-reconstruction. *Earth Planet. Sci. Lett.* **364**, 111–122.

Henehan M. J., Foster G. L., Bostock H. C., Greenop R., Marshall B. J. and Wilson P. A. (2016) A new boron isotope-pH calibration for *Orbulina universa*, with implication for understanding and accounting for 'vital effects'. *Earth Planet. Sci. Lett.* **454**, 282–292.

Hemming N. G. and Hanson G. N. (1992) Boron isotopic composition and concentration in modern marine carbonates. *Geochim. Cosmochim. Acta* **56**, 537–543.

Holcomb M., McCorkle D. C. and Cohen A. L. (2010) Long-term effects of nutrient and CO_2 enrichment on the temperate coral *Astrangia poculata* (Ellis and Solander, 1786). *J. Exp. Mar. Biol. Ecol.* **386**, 27–33.

Holmer L. E. and Popov L. E. (1996) Early Paleozoic radiation and classification of organo-phosphatic brachiopods. In Brachiopods: Proceedings of the Third International Brachiopod Congress Sudbury 1995 (eds. P. Copper and J. Jin). Canada. pp. 117–121.

Hönisch B., Hemming N. G., Grottoli A. G., Amat A., Hanson G. N. and Bijima J. (2004) Assessing scleractinian corals as recorders for paleo-pH: empirical calibration and vital effects. *Geochim. Cosmochim. Acta* **68**, 3675–3685.

Jantzen C., Häussermann V., Försterra G., Laudien J., Adelan M., Maier S. and Richter C. (2013) Occurrence of a cold-water coral along natural pH gradients (Patagonia, Chile). *Mar. Biol.* **160**, 2597–2607.

Joachimski M. M., Simon L., van Geldern R. and Lécuyer C. (2005) Boron isotope geochemistry of Paleozoic brachiopod calcite: Implications for a secular change in the boron isotope geochemistry of seawater over the Phanerozoic. *Geochim. Cosmochim. Acta* **69**, 4035–4044.

Jurikova H., Liebetrau V., Raddatz J., Fietzke J., Trotter J., Rocholl A., Krause S., McCulloch M., Rüggeberg A. and Eisenhauer A. (2019) Boron isotope composition of the cold-water coral Lophelia pertusa along the Norwegian margin: Zooming into a potential pH-proxy by combing bulk and high-resolution approaches. *Chem. Geol.*. https://doi.org/10.1016/j.chemgeo.2019.01.005.

Kaczmarek K., Nehrke G., Misra S., Bijima J. and Elderfield H. (2016) Investigating the effects of growth rate and temperature on the B/Ca ratio and $\delta^{11}B$ during inorganic calcite formation. *Geochim. Cosmochim. Acta* **421**, 81–92.

Kakihana H., Kotaka M., Satoh S., Nomura M. and Okamoto M. (1977) Fundamental studies on the ion-exchange separation of boron isotopes. *Chem. Soc. Jpn. B* **50**, 158–163.

Khalifah R. G. (1971) The carbon dioxide hydration activity of carbonic anhydrase I. Stop-flow kinetic studies on the native human isoenzymes B and C. *J. Biol. Chem.* **246**(8), 2561–2573.

Kiss E. (1988) Ion-exchange separation and spectrophotometric determination of boron in geological materials. *Anal. Chim. Acta* **211**, 243–256.

Klochko K., Kaufman A. J., Wengsheng Y., Byrne R. H. and Tossell J. A. (2006) Experimental measurement of boron isotope fractionation in seawater. *Earth Planet. Sci. Lett.* **248**, 276–285.

Klochko K., Cody G. D., Tossell J. A., Dera P. and Kaufman A. J. (2009) Re-evaluating boron speciation in biogenic calcite and aragonite using ^{11}B MAS NMR. *Geochim. Cosmochim. Acta* **73**, 1890–1900.

Krief S., Hendy E. J., Fine M., Yam R., Meibom A., Foster G. L. and Shemesh A. (2010) Physiological and isotopic responses of scleractinian corals to ocean acidification. *Geochim. Cosmochim. Acta* **74**, 4988–5001.

Kroeker K. J., Kordas R. L., Crim R., Hendriks I. E., Ramajo L., Singh G. S., Duarte C. M. and Gattuso J.-P. (2013) Impacts of ocean acidification on marine organisms: quantifying sensitivities and interaction with warming. *Glob. Chang. Biol.* **19**, 1884–1896.

Lemarchand D., Gaillardet J., Göpel C. and Manhès G. (2002a) An optimized procedure for boron separation and mass spectrometry analysis for river samples. *Chem. Geol.* **182**, 323–334.

Lemarchand D., Gaillardet J., Lewin E. and Allègre C. J. (2002b) Boron isotope systematics in large rivers: implications for the marine boron budget and paleo-pH reconstruction over the Cenozoic. *Chem. Geol.* **190**, 123–140.

Lécuyer C., Grandjean P., Reynard B., Albarède F. and Telouk P. (2002) $^{11}B/^{10}B$ analysis of geological materials by ICP-MS Plasma 54: application to the boron fractionation between brachiopod calcite and seawater. *Chem. Geol.* **186**, 45–55.

Liebetrau V., Augustin N., Kutterolf S., Schmidt M., Eisenhauer A., Garbe-Schönberg D. and Weinrebe W. (2014) Cold-seep-driven carbonate deposits at the Central American forearc: contrasting evolution and timing in escarpment and mound settings. *Int. J. Earth Sci.* **103**, 1845–1872.

Logan A. (2004) Ecological, reproductive and ontogenetic features in *Pajaudina atlantica* Logan (Thecideidae, Brachiopoda, Recent) from the Canary Islands. *Mar. Ecol.* **25**, 207–215.

McCammon H. M. (1973) The ecology of *Magellania venosa*, an articulate brachiopod. *J. Paleontol.* **47**, 266–279.

Mavromatis V., Montouillout V., Noireaux J., Gaillardet J. and Schott J. (2015) Characterization of boron incorporation and speciation in calcite and aragonite from co-precipitation experiments under controlled pH, temperature and precipitation rate. *Geochim. Cosmochim. Acta* **150**, 299–313.

McCulloch M., Falter J., Trotter J. and Montagna P. (2012a) Coral resilience to ocean acidification and global warming through pH up-regulation. *Nat. Clim. Change* **2**, 623–627.

McCulloch M., Trotter J., Montagna P., Falter J., Dunbar R., Freiwald A., Försterra G., López Correa M., Maier C., Rüggeberg A. and Taviani M. (2012b) Resilience of cold-water scleractinian corals to ocean acidification: boron isotopic systematics of pH and saturation state up-regulation. *Geochim. Cosmochim. Acta* **87**, 21–34.

Martínez-Botí M. A., Marino G., Foster G. L., Ziveri P., Henehan M. J., Rae J. W. B., Mortyn P. G. and Vance D. (2015) Boron isotope evidence for oceanic carbon dioxide leakage during the last glaciation. *Nature* **518**, 219–222.

Moya A., Tambutté S., Bertucci A., Tambutté E., Lotto S., Vullo D., Supuran C. T., Allemand D. and Zoccola D. (2008) Carbonic anhydrase in the Scleractinian coral *Stylophora pistillata*. *J. Biol. Chem.* **283**, 25475–25484.

Noireaux J., Mavromatis V., Gaillardet J., Schrott J., Montouillout V., Louvat P., Rollion-Bard C. and Neuville D. R. (2015) Crystallographic control on the boron isotope paleo-pH proxy. *Earth Planet. Sci. Lett.* **430**, 398–407.

Okai T., Suzuki A., Kawahata H., Terashima S. and Imai N. (2002) Preparation of a new geological survey of Japan geochemical reference material: coral JCp-1. *Geostand. Geoanalytical Res.* **26**, 95–99.

Pagani M., Lemarchand D., Spivack A. and Gaillardet J. (2005) A critical evaluation of the boron isotope pH-proxy: the accuracy of ancient ocean pH estimates. *Geochim. Cosmochim. Acta* **69**, 953–961.

Pantoja S., Iriarte J. L. and Daneri G. (2011) Oceanography of the Chilean Patagonia. *Cont. Shelf Res.* **31**, 149–153.

Paris G., Gaillardet J. and Louvat P. (2010) Geological evolution of seawater boron isotopic composition recorded in evaporates. *Geology* **38**, 1035–1038.

Pavlova G. Y., Tishchenko P. Y., Volkova T. I., Dickson A. and Wallmann K. (2008) Intercalibration of Bruevich's method to determine the total alkalinity in seawater. *Oceanology* **48**(3), 438–443.

Penman D. E., Hönisch B., Rasbury E. T., Hemming N. G. and Spero H. J. (2013) Boron, carbon, and oxygen isotopic composition of brachiopod shells: Intra-shell variability, controls, and potential as a paleo-pH recorer. *Chem. Geol.* **340**, 32–39.

Raddatz J., Rüggeberg A., Flögel S., Hathorne E. C., Liebetrau V., Eisenhauer A. and Dullo W.-C. (2014) The influence of seawater pH on U/Ca rations in the scleractinian cold-water coral *Lophelia pertusa*. *Biogeosciences* **11**, 1863–1871.

Ramesh K., Hu M. Y., Thomsen J., Bleich M. and Melzner F. (2017) Mussel larvae modify calcifying fluid carbonate chemistry to promote calcification. *Nat. Comm.* **8**, 1709. https://doi.org/10.1038/s41467-017-01806-8.

Reynaud S., Leclercq N., Romaine-Lioud S., Ferrier-Pagés C., Jaubert J. and Gattuso J.-P. (2003) Interacting effects of CO_2 partial pressure and temperature on photosynthesis and calcification in a scleractinian coral. *Glob. Chang. Biol.* **9**, 1660–1668.

Reynaud S., Hemming N., Juillet-Leclerc A. and Gattuso J.-P. (2004) Effect of pCO_2 and temperature on the boron isotopic composition of the zooxanthellate coral *Acropora* sp.. *Coral Reefs* **23**, 539–546.

Riascos J., Guzmán N., Laudien J., Heilmayer O. and Oliva M. (2007) Suitability of three stains to mark shells of *Concholepas concholepas* (Gastropoda) and *Mesodesma donacium* (Bivalvia). *J. Shellfish Res.* **26**, 43–49.

Ries J. B., Cohen A. L. and McCorkle D. C. (2009) Marine calcifiers exhibit mixed responses to CO_2-induced ocean acidification. *Geology* **39**, 1131–1134.

Rollion-Bard C., Chaussidon M. and France-Lanord C. (2003) pH control on oxygen isotopic composition of symbiotic corals. *Earth Planet. Sci. Lett.* **215**, 275–288.

Rollion-Bard C. and Erez J. (2010) Intra-shell boron isotope ratios in the symbiont-bearing benthic foraminiferan *Amphistegina lobifera*: Implications for $\delta^{11}B$ vital effects and paleo-pH reconstructions. *Geochim. Cosmochim. Acta* **74**, 1530–1536.

Rollion-Bard C., Cuif J.-P. and Blamart D. (2017) Optical observation and geochemical data in Deep-Sea Hexa- and Octo-Coralla specimens. *Minerals* **7**, 154–175.

Romanin M., Crippa G., Ye F., Brand U., Bitner M. A., Gaspard D., Häussermann V. and Laudien J. (2018) A sampling stategy for recent and fossil brachiopods: selecting the optimal shell segment for geochemical analyses. *Riv. It. Paleontol. Strat.* **124**, 343–359.

Ross C. L., Schoepf V., DeCarlo T. M. and McCulloch M. T. (2018) Mechanisms and seasonal drivers of calcification in the temperate coral *Turbinaria reniformis* at its latitudinal limits. *Proc. R. Soc. B.* **285**, 20180215.

Sanyal A., Nugent M., Reeder R. J. and Bijima J. (2000) Seawater pH control on the boron isotopic composition of calcite: Evidence from inorganic calcite precipitation experiments. *Geochim. Cosmochim. Acta* **64**, 1551–1555.

Sievers H. A. and Silva N. (2008a) Dissolved oxygen, pH, and nutrients in the austral Chilean channels and fjords. In *Progress in the Oceanographic Knowledge of Chilean Interior Waters, from Puerto Montt to Cape Horn* (eds. H. A. Sievers and N. Silva). Comité Oceanográfico Nacional–Pontificia Universidad Católica de Valparaíso, Valparaíso, pp. 37–48.

Sievers H. A. and Silva N. (2008b) Temperature and salinity in the austral Chilean channels and fjords. In *Progress in the Oceanographic Knowledge of Chilean Interior Waters, from Puerto Montt to Cape Horn* (eds. H. A. Sievers and N. Silva). Comité Oceanográfico Nacional-Pontificia Universidad Católica de Valparaíso, Valparaíso, pp. 31–36.

Sievers H. A. and Silva N. (2008c) Water masses and circulation in austral Chilean channels and fjords. In *Progress in the Oceanographic Knowledge of Chilean Interior Waters, from Puerto Montt to Cape Horn* (eds. H. A. Sievers and N. Silva). Comité Oceanográfico Nacional–Pontificia Universidad Católica de Valparaíso, Valparaíso, pp. 53–58.

Silverman J., Lazar B., Cao L., Caldeira K. and Erez J. (2009) Coral reefs may start dissolving when atmospheric CO_2 doubles. *Geophys. Res. Lett.* **36**, L05606. https://doi.org/10.1029/2008GL036282.

Stewart J. A., Anagnostou E. and Foster G. L. (2016) An improved isotope pH proxy calibration for the deep-sea coral *Desmophyllum dianthus* through sub-sampling of fibrous aragonite. *Chem. Geol.* **447**, 148–160.

Stumpp M., Hu M. Y., Melzner F., Gutowska M. A., Dorey N., Himmerkus N., Holtmann W. C., Dupont S. T., Thorndyke M. C. and Bleich M. (2012) Acidified seawater impacts sea urchin larvae pH regulatory systems relevant for calcification. *Proc. Natl. Acad. Sci.* **109**, 18192–18197.

Stumpp M., Hu M. Y., Casties I., Saborowski R., Bleich M., Melzner F. and Dupont S. (2013) Digestion in sea urchin larvae impaired under ocean acidification. *Nat. Clim. Change* **3**, 1044–1049.

Stumpp M., Hu M. Y., Tseng Y.-C., Guh Y.-J., Chen Y.-C., Yu J.-K., Su Y.-H. and Hwang P.-P. (2015) Evolution of extreme stomach pH in bilateria inferred from gastric alkalization mechanisms in basal deuterostomes. *Sci. Rep.* **5**, 10421. https://doi.org/10.1038/srep10421.

Taubner I., Böhm F., Eisenhauer A., Tambutté E., Tambutté S., Moldzio S. and Bleich M. (2017) An improved approach investigating epithelial ion transport in scleractinian corals. *Limnol. Oceanogr. Methods* **15**, 753–765.

Tanaka K., Holcomb M., Takahashi A., Kurihara H., Asami R., Shinjo R., Sowa K., Rankenburg K., Watanabe T. and McCulloch M. (2015) Response of *Acropora digitifera* to ocean acidification: constraints from $\delta^{11}B$, Sr, Mg and Ba composition of aragonitic skeletons cultured under variable seawater pH. *Coral Reefs* **34**, 1139–1149.

Trotter J., Montagna P., McCulloch M., Silenzi S., Reynaud S., Mortimer G., Martin S., Ferrier-Pages C., Gattuso J.-P. and Rodolfo-Metalpa R. (2011) Quantifying the pH 'vital effect' in the temperate zooxanthellate coral *Cladocora caespitosa*: validations of the boron seawater pH proxy. *Earth Planet. Sci. Lett.* **303**, 163–173.

Uchikawa J., Penman D. E., Zachos J. C. and Zeebe R. E. (2015) Experimental evidence for kinetic effects on B/Ca in synthetic calcite: Implications for potential $B(OH)_4^-$ and $B(OH)_3$ incorporation. *Geochim. Cosmochim. Acta* **150**, 171–191.

Veizer J., Ala D., Azmy K., Bruckschen P., Buhl D., Bruhn F., Carden G. A. F., Diener A., Ebneth S., Godderis Y., Jasper T., Korte C., Pawellek F., Podlaha O. G. and Strauss H. (1999) $^{87}Sr/^{86}Sr$, $\delta^{13}C$ and $\delta^{18}O$ evolution of Phanerozoic seawater. *Chem. Geol.* **161**, 59–88.

Venn A. A., Tambutté E., Holcomb M., Laurent J., Allemand D. and Tambutté S. (2013) Impact of seawater acidification on pH at the tissue-skeleton interfacte and calcification in reef corals. *Proc. Natl. Acad. Sci.* **110**, 1634–1639.

Vengosh A., Kolodny Y., Starinsky A., Chivas A. R. and McCulloch M. T. (1991) Coprecipitation and isotopic fractionation of boron in modern biogenic carbonates. *Geochim. Cosmochim. Acta* **55**, 2901–2910.

Vollstaedt H., Eisenhauer A., Wallmann K., Böhm F., Fietzke J., Liebetrau V., Krabbenhöft A., Farkaš J., Tomašovych A., Raddatz J. and Veizer J. (2014) The Phanerozoic $\delta^{88/86}Sr$ record of seawater: new constraints on past changes in oceanic carbonate fluxes. *Geochim. Cosmochim. Acta* **128**, 249–265.

Vogl J. and Rosner M. (2001) Production and certification of a unique set of osotope and delta reference materials for boron isotope determination in geochemical, environmental and industrial materials. *Geostand. Geoanalytical Res.* **36**, 161–175.

Wall M., Ragazzola F., Foster L. C., Form A. and Schmidt D. N. (2015) pH up-regulation as a potential mechanisms for the cold-water coral *Lophelia pertusa* to sustain growth in aragonite undersaturated conditions. *Biogeosciences* **12**, 6869–6880.

Wall M., Fietzke J., Schmidt G. M., Fink A., Hofmann L. C., de Beer D. and Fabricius K. E. (2016) Internal pH regulation facilitates in situ long-term acclimation of massive corals to end-of-century carbon dioxide conditions. *Sci. Rep.* **6**, 30688. https://doi.org/10.1038/srep30688.

Williams A. (1966) Growth and structure of the shell of living articulate brachiopods. *Nature* **211**, 1146–1148.

Ye F., Crippa G., Angiolini L., Brand U., Capitani G., Cusack M., Garbelli C., Griesshaber E., Harper E. and Schmahl W. (2018) Mapping of recent brachiopod microstructure: a tool for environmental studies. *J. Struct. Biol.* **201**, 221–236. https://doi.org/10.1016/j.jsb.2017.11.011.

Zeebe R. E. (2005) Stable boron isotope fractionation between dissolved $B(OH)_3$ and $B(OH)_4^-$. *Geochim. Cosmochim. Acta* **69**, 2753–2766.

Zeebe R. E. and Wolf-Gladrow D. A. (2001) CO_2 in seawater: equilibrium, kinetics, isotopes. In *Elsevier Oceanography Series 65*. Elsevier, p. 346.

Zeebe R. E., Sanyal A., Ortiz J. D. and Wolf-Gladrow D. A. (2001) A theoretical study of the kinetics of the boric acid-borate equilibrium in seawater. *Mar. Chem.* **73**, 113–124.

Associate editor: James Farquhar